Submarine deposits from pumiceous pyroclastic density currents traveling over water

Jutzeler, M.; Manga, M.; White, J.d.l.; Talling, P.j.; Proussevitch, A.a.; Watt, S.f.l.; Cassidy, M.; Taylor, R.n.; Le Friant, A.; Ishizuka, O.

DOI:
10.1130/B31448.1

THE GEOLOGICAL SOCIETY OF AMERICA®

Submarine deposits from pumiceous pyroclastic density currents traveling over water: An outstanding example from offshore Montserrat (IODP 340)

M. Jutzeler[1,2,3,†], M. Manga[4], J.D.L. White[2], P.J. Talling[1], A.A. Proussevitch[5], S.F.L. Watt[6], M. Cassidy[7], R.N. Taylor[8], A. Le Friant[9], and O. Ishizuka[10]

[1]*National Oceanography Centre, Southampton SO14 3ZH, UK*
[2]*Department of Geology, University of Otago, Dunedin 9054, New Zealand*
[3]*School of Physical Sciences and Centre of Excellence in Ore Deposits (CODES), University of Tasmania, Hobart TAS 7001, Australia*
[4]*Department of Earth and Planetary Science, University of California, Berkeley, California 94720, USA*
[5]*Climate Change Research Center, University of New Hampshire, Durham, New Hampshire 03824, USA*
[6]*School of Geography, Earth and Environmental Sciences, University of Birmingham, Birmingham B15 2TT, UK*
[7]*Institute of Geosciences, Johannes Gutenberg University, 55128 Mainz, Germany*
[8]*School of Ocean and Earth Science, University of Southampton, Southampton SO14 3ZH, UK*
[9]*Institut de Physique du Globe de Paris, Université Paris Diderot, 75238 Paris, France*
[10]*Geological Survey of Japan, National Institute of Advanced Industrial Science and Technology (AIST), Ibaraki 305-8567, Japan*

ABSTRACT

Pyroclastic density currents have been observed to both enter the sea, and to travel over water for tens of kilometers. Here, we identified a 1.2-m-thick, stratified pumice lapilli-ash cored at Site U1396 offshore Montserrat (Integrated Ocean Drilling Program [IODP] Expedition 340) as being the first deposit to provide evidence that it was formed by submarine deposition from pumice-rich pyroclastic density currents that traveled above the water surface. The age of the submarine deposit is ca. 4 Ma, and its magma source is similar to those for much younger Soufrière Hills deposits, indicating that the island experienced large-magnitude, subaerial caldera-forming explosive eruptions much earlier than recorded in land deposits. The deposit's combined sedimentological characteristics are incompatible with deposition from a submarine eruption, pyroclastic fall over water, or a submarine seafloor-hugging turbidity current derived from a subaerial pyroclastic density current that entered water at the shoreline. The stratified pumice lapilli-ash unit can be subdivided into at least three depositional units, with the lowermost one being clast supported. The unit contains grains in five separate size modes and has a >12 phi range. Particles are chiefly subrounded pumice clasts, lithic clasts, crystal fragments, and glass shards. Pumice clasts are very poorly segregated from other particle types, and lithic clasts occur throughout the deposit; fine particles are weakly density graded. We interpret the unit to record multiple closely spaced (<2 d) hot pyroclastic density currents that flowed over the ocean, releasing pyroclasts onto the water surface, and settling of the various pyroclasts into the water column. Our settling and hot and cold flotation experiments show that waterlogging of pumice clasts at the water surface would have been immediate. The overall poor hydraulic sorting of the deposit resulted from mixing of particles from multiple pulses of vertical settling in the water column, attesting to complex sedimentation. Slow-settling particles were deposited on the seafloor together with faster-descending particles that were delivered at the water surface by subsequent pyroclastic flows. The final sediment pulses were eventually deflected upon their arrival on the seafloor and were deposited in laterally continuous facies. This study emphasizes the interaction between products of explosive volcanism and the ocean and discusses sedimentological complexities and hydrodynamics associated with particle delivery to water.

INTRODUCTION

Pumice-rich volcaniclastic deposits are widely recognized in the marine record. They may originate via pyroclastic density currents entering or traveling over water, pyroclastic fall onto water, submarine eruptions, or by resedimentation (e.g., Cas and Wright, 1991; McPhie et al., 1993; Carey, 2000; Kano, 2003; Manville et al., 2010). In addition to their volcanological significance and substantial effects on marine benthic life (Wiesner et al., 1995; Wetzel, 2009), they are broadly important in geological studies because they are commonly deposited as widespread blankets on the seafloor, which makes them excellent chronostratigraphic markers (Lowe, 2011; Larsen et al., 2014). Furthermore, these voluminous accumulations of pyroclasts record large-scale explosive eruptions of the sort that pose geological hazards for coastal populations (e.g., Carey et al., 1996; Mastin and Witter, 2000; Kano, 2003; Manville et al., 2010). Here, we document an anomalous deposit cored at Site U1396 of Integrated Ocean Drilling Program (IODP) Expedition 340 offshore Montserrat (Lesser Antilles; Expedition 340 Scientists, 2012). This stratified pumice lapilli-ash unit, which formed at ca. 4 Ma, has textural characteristics, in particular stratification, sorting, and grading, that are dissimilar to those of previously described submarine volcaniclastic facies. It is much thicker (1.2 m) than other volcaniclastic units at the same site (Expedition 340 Scientists, 2012; Wall-Palmer et al., 2014), and it contains abundant highly compositionally evolved pumice clasts.

We used flotation and settling column experiments and assessment of multiple deposit features (stratigraphy, grain size, componentry, microtomography, and pumice vesicularity) to

†Present address: School of Physical Sciences (Earth Sciences), University of Tasmania, Private Bag 79, Hobart TAS 7001, Australia; jutzeler@gmail.com.

doi: 10.1130/B31448.1; 16 figures; 1 table; Data Repository item 2016253.

investigate the nature of particle transport for this unit. Based on facies characteristics that do not match those from other transport processes, we argue that this unit is the product of a two-step transport process involving multiple dilute pyroclastic density currents that traveled tens of kilometers over the sea surface, coupled with quick waterlogging and settling of pyroclasts that were delivered to the water surface and then settled through the water column in multiple sedimentation pulses. This mechanism of sedimentation has been witnessed, reproduced, and modeled (Lacroix, 1904; Sigurdsson et al., 1982; Cas and Wright, 1991; Fisher et al., 1993; Carey et al., 1996; Allen and Cas, 2001; Freundt, 2003; Dufek et al., 2007; Maeno and Taniguchi, 2007; Trofimovs et al., 2006, 2008, 2012), yet associated submarine pumice-rich deposits have not been previously identified, studied, or sampled. We used geochemistry, including Pb isotopes, to infer a Montserrat Island source for the deposit.

Novel aims of this study are: (1) to characterize a style of marine volcaniclastic facies generated by common eruption and transport mechanisms, but which have not previously been sampled *in situ*; (2) to improve knowledge of eruption and transport processes leading to formation of marine tephra beds; (3) to investigate the behavior of pumice in water, in particular, pumice waterlogging, which is highly significant in marine volcanology; and (4) to provide a better record of the volcanism, geochemistry, and time of emergence for Montserrat Island, and thus enhance our understanding of the growth rates of volcanic islands and of the potential for catastrophic eruptions in island arcs generally. This study presents critical data on complex transport processes associated with coastal volcanism, and it is relevant to assessment of hazards to distant coastal populations and shipping. Moreover, it has implications for the dispersal of pyroclasts over and in the ocean, and it directly addresses a way of forming thick ash beds on the seafloor. Experiments on rates of waterlogging for pumice reported in this study have broad implications for formation of water-laden ash beds, faunal dispersal, and maritime hazards (Bryan et al., 2012; Jutzeler et al., 2014a).

Sources of Pumice-Rich Deposits

In coastal settings, subaerial pyroclastic density currents commonly reach shorelines and interact with seawater. Upon meeting the water, pyroclastic density currents may flow directly into or under the water and deposit all or part of their sediment near the shore, building a delta (e.g., Trofimovs et al., 2008), and/or they may separate into two parts, with dense clast-rich basal parts of currents feeding water-supported, seafloor-hugging density currents, while their upper parts travel over the sea as dilute pyroclastic density currents, until they lose energy (Carey et al., 1996; Allen and Cas, 2001; Dufek et al., 2007; Maeno and Taniguchi, 2007; Trofimovs et al., 2008). Subaerial overwater pyroclastic density currents and subaqueous turbidity currents can both transport pumice clasts for at least tens of kilometers offshore (Lacroix, 1904; Sigurdsson et al., 1982; Cas and Wright, 1991; Cole and DeCelles, 1991; Fisher et al., 1993; Carey et al., 1996; White, 2000; Allen and Cas, 2001; Freundt, 2003; Dufek et al., 2007; Maeno and Taniguchi, 2007; Allen et al., 2012; Schindlbeck et al., 2013; Kutterolf et al., 2014). A few pyroclastic density currents have been witnessed traveling over water (Lacroix, 1904; Simkin and Fiske, 1983; Swanson and Kienle, 1988; Carey et al., 1996; Cole et al., 1998; Hart et al., 2004). Several on-land exposures separated from their vents by ocean waters show that voluminous pumice-rich pyroclastic density currents can travel over water and retain their heat for tens of kilometers. The Ito pyroclastic density current (Aira caldera, Japan; Yokoyama, 1974) traveled more than 20 km over water; the Campanian ignimbrite current (Phlegrean Fields, Italy; Fisher et al., 1993) traveled 35 km; the current that formed the Kos Plateau Tuff (Kos, Greece; Allen and Cas, 2001) traveled 35 km (possibly 60 km); the Koya ignimbrite-forming current (Kikai caldera, Japan; Ui, 1973; Maeno and Taniguchi, 2007) traveled >50 km; and the pyroclastic density current that deposited the Krakatau ignimbrite (Indonesia; Carey et al., 1996) traveled 65–80 km. Pumiceous pyroclastic density currents reaching a water body may choke the coastal water surface with floating clasts and thus provide a solid surface on which succeeding pumice clasts can accumulate above water and be slowly air-cooled before touching seawater. Such a pumice raft temporarily extending the shore can facilitate offshore dispersal, notably of lithic clasts (Burgisser, 2005; Dufek and Bergantz, 2007; Dufek et al., 2009), and can enhance runout of subsequent pyroclastic density currents (Self, 1992). Pyroclastic pumice fallout from an atmospheric plume can drop a large amount of air-cooled pumice clasts onto the ocean (Watkins et al., 1978; Ledbetter and Sparks, 1979), where they accumulate in floating rafts (Bryan et al., 2012; Jutzeler et al., 2014a), eventually dispersed by ocean surface currents so that the pumice clasts either sink to the seafloor or get stranded along coastlines. Pumice-rich submarine deposits can also be formed when pumice is delivered directly into the ocean by underwater eruptions, with much or all of this material having no interaction with the atmosphere (Cas and Wright, 1991; Kano, 2003; Allen and McPhie, 2009; Carey et al., 2014; Jutzeler et al., 2014b, 2015a). Pumice clasts can also be resedimented in fluvial and coastal environments, and eventually enter the ocean as already-waterlogged pumice, or as floating clasts that form pumice rafts (Manville et al., 1998, 2002; Riggs et al., 2001; Kataoka and Nakajo, 2002; Kataoka, 2005; Larsen et al., 2014). Settling through the water column leads to hydraulic sorting (Jutzeler et al., 2015b) of the clasts by their drag (i.e., clast size, density, and shape). Water settling of large volumes of volcanic clasts can form vertical plumes of fine ash (Manville and Wilson, 2004; Jacobs et al., 2015). Volcaniclastic deltas formed by eruptions or resedimentation may then be destroyed by coastal erosion and/or mass wasting, generating subsequent density currents (Allen and Freundt, 2006; Trofimovs et al., 2008).

Behavior of Pumice in Water

Pumice clasts are chiefly generated by explosive eruptions and occur in most depocenters surrounding arc volcanoes. The abundance of pumice clasts on the seafloor and in the submarine geological record testifies to their ability to waterlog and sink (Carey and Sigurdsson, 1980; Nishimura, 1991; Mandeville et al., 1996; Fiske et al., 1998, 2001; Carey, 2000; Kano, 2003; Tani et al., 2008; Allen and McPhie, 2009; Allen et al., 2010; Schindlbeck et al., 2013; Jutzeler et al., 2014b, 2014c; Kutterolf et al., 2014; Larsen et al., 2014). It is well known that dry, cold pumice can float in water, because of its low density and relatively low permeability (Whitham and Sparks, 1986; Klug and Cashman, 1996; White et al., 2001; Bryan et al., 2012; Jutzeler et al., 2014a). In contrast, hot (>boiling temperature) pumice clasts up to lapilli in size are known to almost immediately sink upon contact with water (Whitham and Sparks, 1986; Dufek et al., 2007; Allen et al., 2008).

The precise mechanisms associated with the ingestion of water into the pumice pores at the expense of a gas phase (air, magmatic gas) remain incompletely understood. Simple flotation experiments can re-create conditions of pumice waterlogging, allowing inferences to be made about the transport and sedimentation behaviors associated with submarine pumice-rich deposits. Few results of flotation experiments have been published, although the unusual interaction of pumice with water has caught the attention of scientists for centuries (e.g., van Leuwenhock, 1704; Whitham and Sparks, 1986; Campbell et al., 1987; Manville et al., 1998, 2002; White et al., 2001; Risso et al.,

2002; Dufek et al., 2007; Vella and Huppert, 2007; Allen et al., 2008).

In contact with external water, a hot pumice clast (i.e., at temperature above the boiling point) will quench and waterlog in a matter of seconds for grain sizes up to lapilli size (Whitham and Sparks, 1986; Kato, 1987; Dufek et al., 2007; Allen et al., 2008). Cooling of the pumice clast condenses the steam present in its vesicle network, creating an underpressure that draws water inward, effectively quenching and waterlogging the pumice. The efficiency of waterlogging in hot pumices clasts has been related to clast temperature (Whitham and Sparks, 1986), porosity, permeability (Whitham and Sparks, 1986; Allen et al., 2008), and size (Dufek et al., 2007). Complex rates of waterlogging occur around the Leidenfrost temperature (150–300 °C; Campbell et al., 1987), and highly vesicular pumice clasts may need to be at temperatures exceeding 300 °C to immediately sink in water (Whitham and Sparks, 1986). In contrast, a cold pumice waterlogs by capillarity, which can delay waterlogging by years (Whitham and Sparks, 1986; White et al., 2001; Manville et al., 2002; Vella and Huppert, 2007; Bryan et al., 2012), although models for capillary infiltration greatly underestimate the waterlogging time (Vella and Huppert, 2007). Cold pumice waterlogging time has been shown in some experiments to be related to the size of the clast (Whitham and Sparks, 1986; White et al., 2001; Risso et al., 2002).

GEOLOGICAL SETTING AND IODP SAMPLES

Montserrat Island is part of the Lesser Antilles island arc (Briden et al., 1979; Bouysse and Westercamp, 1990). It is ~100 km^2 and consists of four volcanic centers (Fig. 1) that have produced predominantly andesitic material. On-land ages are younger southward, with Silver Hills (2600–1200 ka) to the north, Centre Hills (950–550 ka) in the middle, and the South-Soufrière Hills and Soufrière Hills complexes (174 ka to present) to the south (Rea, 1974; Harford et al., 2002; Zellmer et al., 2003; Cassidy et al., 2015). Ongoing dome growth and collapse at Soufrière Hills have occurred since 1995 (Young et al., 1998; Robertson et al., 2000).

Multiple marine expeditions have been dedicated to studying the seafloor bathymetry and shallow crust around the island, allowing identification of volcaniclastic and debris avalanche deposits (Deplus et al., 2001; Boudon et al., 2007; Le Friant et al., 2008; Trofimovs et al., 2010, 2013; Lebas et al., 2011; Watt et al., 2012a, 2012b; Cassidy et al., 2013, 2014a, 2014b, 2015; Le Friant et al., 2015; Watt et al., 2015; Coussens et al., 2016). Before the IODP 340 Expedition, coring offshore Montserrat was restricted to shallow piston cores or vibrocores characterizing volcanic eruptions and mass wasting events of Soufrière Hills and South-Soufrière Hills extending back to ca. 110 ka (Le Friant et al., 2008; Trofimovs et al., 2013; Cassidy et al., 2013, 2014a, 2014b; Watt et al., 2015).

In 2012, Site U1396 was drilled 35 km to the southwest of Montserrat (16°30.49N, 62°27.10W) during the IODP 340 Expedition (Expedition 340 Scientists, 2012). This site is located on a bathymetric high and is characterized by laterally continuous seismic reflectors (Expedition 340 Scientists, 2012). It was chosen for tephra chronology because its elevated position (787 m below seafloor [mbsf]) helped to avoid thick debris avalanche and density current deposits (Expedition 340 Scientists, 2012; Wall-Palmer et al., 2014), which are difficult to core (Jutzeler et al., 2014d). Successful piston coring (APC; Jutzeler et al., 2014d) down to ~140 mbsf in two holes (U1396A and U1396C), separated laterally by 40 m, produced by far the best-preserved and best-recovered cores (0.8% and 3% of the cores were disturbed, respectively) of the entire expedition (Expedition 340 Scientists, 2012; Jutzeler et al., 2016). The cores consist of hemipelagic mud interbedded with ~171 volcaniclastic intervals inferred to have formed mostly by fallout from subaerial eruption plumes onto water. The stratified pumice lapilli-ash, the unit of interest to this study, occurs near the bottom of the holes at ~123 mbsf, specifically in core sections U1396A-14H5-14H6 and sections U1396C-14H2-14H3. It is by far the thickest undisturbed volcaniclastic unit seen at this site.

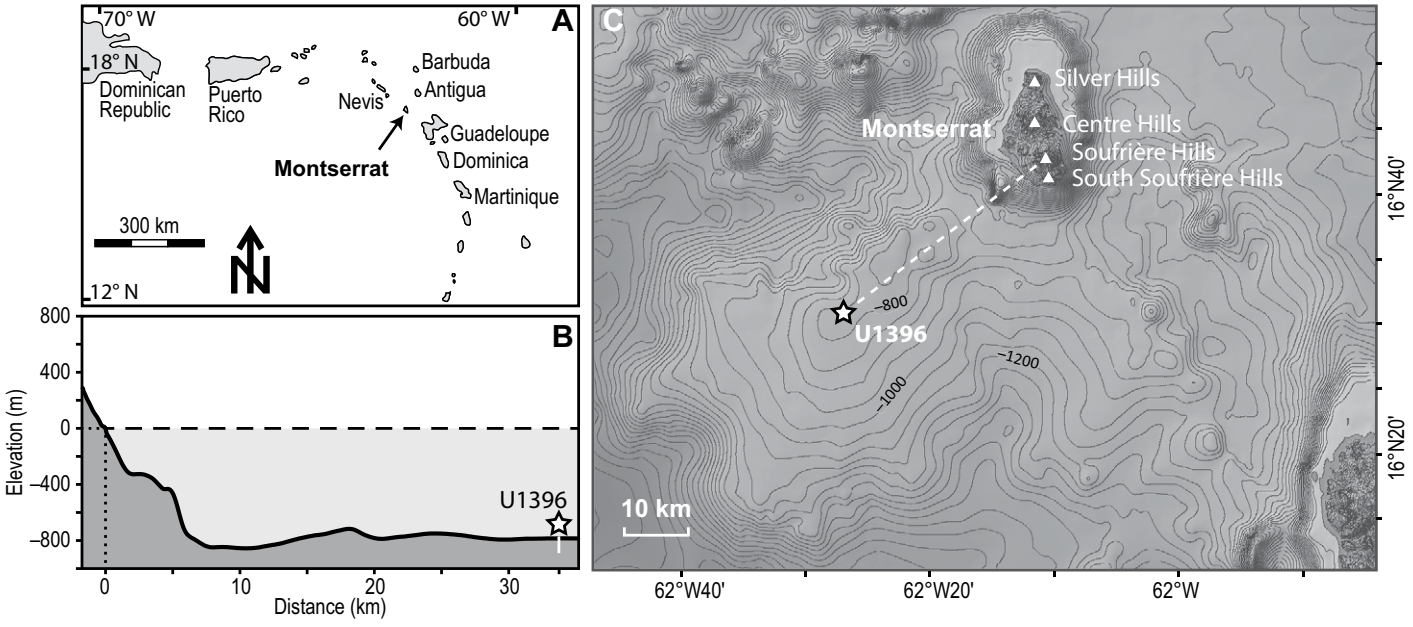

Figure 1. Site U1396 (Integrated Ocean Drilling Program [IODP] 340) offshore Montserrat Island, Lesser Antilles. (A) Location map. (B) Bathymetry profile from Montserrat to Site U1396. (C) Bathymetry and topography around Montserrat, with four main volcanic edifices. Dashed line is projected bathymetry profile in B.

METHODS

Grain-Size Distribution

We calculated grain-size distributions using two techniques. The core samples were dried for 24 h in an oven at 80 °C, split at 710 µm (0.75 phi), and weighed on a high-precision scale. The coarse fraction was dry sieved and weighed at ½ phi intervals. The sub–710 µm fraction was analyzed at ¼ phi using a Malvern laser diffraction particle analyzer at the National Oceanography Centre, Southampton, UK. For this analysis, ~1 cm^3 of sample was dispersed in 30 mL of solution with 0.05% sodium hexametaphosphate. Analyses were run in triplicate and then averaged. The two grain-size distribution data sets are joined at 710 µm, and the bulk weight used for normalization. To avoid artifacts resulting from poorly known differences in density of individual clasts among samples, we present sieve data (in wt%) and laser diffraction data (in vol%) on single graphs normalized by their respective bulk weight. In this paper, grain size is subdivided into coarse (>500 µm), medium (250–500 µm), fine (125–250 µm), very fine (63–125 µm), and extremely fine (<63 µm) ash, following White and Houghton (2006).

Componentry

Componentry was semiquantitatively measured by estimating proportions of each component under a stereomicroscope. Componentry analyses were carried out on three grain size classes (>710 µm, 250–710 µm, 63–250 µm) to allow precise semiquantitative measurements. To avoid discrepancies in estimates of the abundance of different clast types, sample componentry of the entire data set was carried out during a single session. Each sample was analyzed twice (i.e., over two sequences) and cross-compared for consistency. Clast types include: pumice clasts, glass shards, lithic fragments (chiefly nonvesicular/low-vesicularity andesite), ferromagnesian crystals, quartz and feldspar crystals, and foraminifera tests.

Geochemistry—Including Pb Isotopes

Whole-rock geochemical analyses of groups of pumice clasts were carried out by X-ray fluorescence (XRF) at the University of Tasmania, Australia. Glass chemistry analyses were conducted on a Cameca SX-50 electron probe microanalyzer (EPMA) at the University of Bristol, UK, taking specific measures to minimize Na migration in the glass during wavelength-dispersive spectrometry.

Pb isotopes were analyzed for four samples of randomly selected samples from U1396, including small pumice lapilli (two separate samples from U1396A-14H5, 68–70 cm and U1396C-14H3, 85–87 cm), lithic lapilli (from U1396C-14H3, 85–87 cm), and medium to coarse particles (from U1396A-14H5, 138 cm). Samples were prepared following standard procedures in a clean laboratory suite at the University of Southampton, National Oceanography Centre, Southampton, UK (see Table DR1).[1] Pb isotopic compositions were determined on 200 mg of handpicked material that was leached in 4 mL of 6 *M* HCl at 140 °C in sealed Teflon pots for 1 h prior to dissolution in HF-HNO_3. Isolation of Pb from the matrix was performed using AG1-X8 200–400 mesh anion exchange resin. The procedural blanks measured with the samples contained <50 pg of Pb. Pb isotope analyses were conducted on a Neptune multicollector–inductively coupled plasma–mass spectrometer (MC-ICP-MS) at the University of Southampton, with mass fractionation corrected by the double spike technique using the method outlined by Taylor et al. (2015). Pb standard NBS 981 gave results of 16.9408 ± 25 for $^{206}Pb/^{204}Pb$, 15.4975 ± 21 for $^{207}Pb/^{204}Pb$, and 36.7172 ± 66 for $^{208}Pb/^{204}Pb$.

Flotation Experiments

Cold flotation experiments were carried out using 2.5–22 mm pumice clasts at room temperature (20 °C) at the University of Otago, New Zealand. Pumice clasts were cleaned of any small particles on their surface under tap water, then placed in an ultrasonic bath for 15 min, and subsequently dried at 100 °C for 2 d. Once cooled to room temperature, pumice clasts were dropped from a height of a few centimeters onto a 5-cm-wide plastic receptacle filled with tap water, and allowed to sink. Sinking time was recorded by time-lapse digital photography (from 5 s steps initially to 5 min steps after a day), and additional video capture with a digital camera was used for quickly sinking (<2 min) clasts. The flotation time corresponds to the time between when the clast touched the water until it was entirely submerged. Once entirely submerged, all pumice clasts quickly sank to the bottom of the receptacle and remained there. During preliminary floating experiments, small bubbles grew around the immersed parts of the clasts, enhancing their buoyancy (especially the platy clasts), which dramatically increased the flotation time for an individual clast between repeat runs and made the experiments irreproducible. These bubbles originated from slow degassing of tap water and from gas expelled from the clast interior during waterlogging. To mitigate the spurious effect of bubbles, bubbles were continuously removed using a shaking device fixed to the rack that held the samples, making the pumice move gently on the surface of the water to dislodge the trapped bubbles. Several experiments were conducted for each of the pumice clasts, and the selected time corresponds to the shortest flotation time that could be reproduced. The addition of the shaking did not alter the pattern of flotation time, and many clasts floated for the same time with and without shaking. Pumice clasts were left to dry at 60 °C for 24 h between repeat tests.

Hot flotation experiments were conducted at the University of California at Berkeley, California, using the same pumice clasts that were previously used for cold experiments. Pumice clasts were placed in crucibles and heated at 600 °C in a Lindberg furnace for 1 h to reach thermal equilibrium. The crucible containing the clast was then transferred out of the furnace in less than 3 s, with no substantial heat loss (Dufek et al., 2007). The hot pumice clasts were dropped off the crucible into a beaker filled with tap water at 20 °C, and their flotation time was recorded with a high-speed camera at 500 frames per second (fps). As for cold experiments, the flotation time corresponds to the time between when the clast touched the water until it was entirely submerged.

Settling Column Experiment

Settling column experiments were carried out on waterlogged clasts at the National Oceanography Centre, University of Southampton, UK, using a 1.8-m-tall, 20-cm-wide settling column filled with tap water at 20 °C. Settling times were converted into grain-size bins following the Soulsby (1997) settling time equations, using the Matlab® routine "cal_settling" version 1.17 (2005) by Urs Neumeier, available at http://neumeier.perso.ch/matlab/cal_settling.html. All samples were allowed to waterlog for 1 wk before the experiments. The maximum settling time available on the software attached to the settling column is 800 s, which is not enough to allow the smallest particles to reach bottom, and this caused truncation in the distribution of settling times. Settling experiments were carried out on pumice clasts (up to 15 mm), other medium to coarse ash particles, and bulk samples from four intervals through the stratigraphy (U1396A-14H5, 48–50 cm, U1396A-14H5, 108–110 cm, U1396A-14H5, 124–126 cm, and U1396A-14H6, 6–8 cm). The results from runs on the same samples were very similar, so we averaged the results for simplicity.

[1]GSA Data Repository item 2016253, geochemistry dataset, is available at http://www.geosociety.org/pubs/ft2016.htm or by request to editing@geosociety.org.

Pumice Density and Porosity

We measured the density of pumice clasts used for the flotation experiments. The clasts were dried for 24 h at 80 °C and weighed. The clasts were then spray-coated with silicone to make them waterproof and left to dry for a day. The added coat of silicone spray has a negligible weight and volume in water. We used the classical method following Archimedes' principle (Houghton and Wilson, 1989), by comparing the weight of a clast in air versus in water. Porosity was calculated using pumice density data and assuming a dense rock equivalent value of 2400 kg/m^3, matching the density of a rhyolitic aphyric glass (Klug et al., 2002).

Microtomography

Microtomography on pumice clasts was conducted to assess their porosity and vesicle texture, and to check that clasts were not obstructed with foreign material and vesicles were free of any water. Microtomography is a nondestructive, high-resolution method for visualizing contrasts of density in three dimensions. It was carried out on beamline 8.3.2 on the Synchrotron-based Hard X-Ray Micro-Tomography instrument at the Advanced Light Source at the Lawrence Berkeley National Laboratory, University of California at Berkeley, California. Thirteen clasts randomly selected through the entire unit stratigraphy were analyzed at 14–29 keV with 1.3 µm and 3.2 µm voxel size, using 2048 projections, each of them 2560 pixels in width and of variable height.

FACIES ANALYSIS

We carried out detailed stratigraphic and textural analysis of the stratified pumice lapilli-ash at Site U1396 offshore Montserrat (Fig. 1), with a specific focus on grain-size distribution, clast componentry, and roundness and vesicle textures of pumice clasts. This facies analysis included detailed quantitative and qualitative textural description of the bed forms and the clasts, in addition to settling properties of the clasts measured in settling experiments and an independent calculation of the deposit's hydraulic sorting.

Stratified Pumice Lapilli-Ash

The stratified pumice lapilli-ash was recovered in Holes U1396A (122.36–123.51 mbsf) and U1396C (123.04–124.3 mbsf). The unit was seen in sections U1396A-14H5-14H6 and sections U1396C-14H2-14H3 (Fig. 2), and it has an age of ca. 4 Ma from micropaleontology and paleomagnetic data (Expedition 340 Scientists, 2012; Le Friant et al., 2015). The unit is in sharp contact with underlying and overlying intervals of hemipelagic mud. Several ash layers interbedded with the hemipelagic mud below and above the stratified pumice lapilli-ash

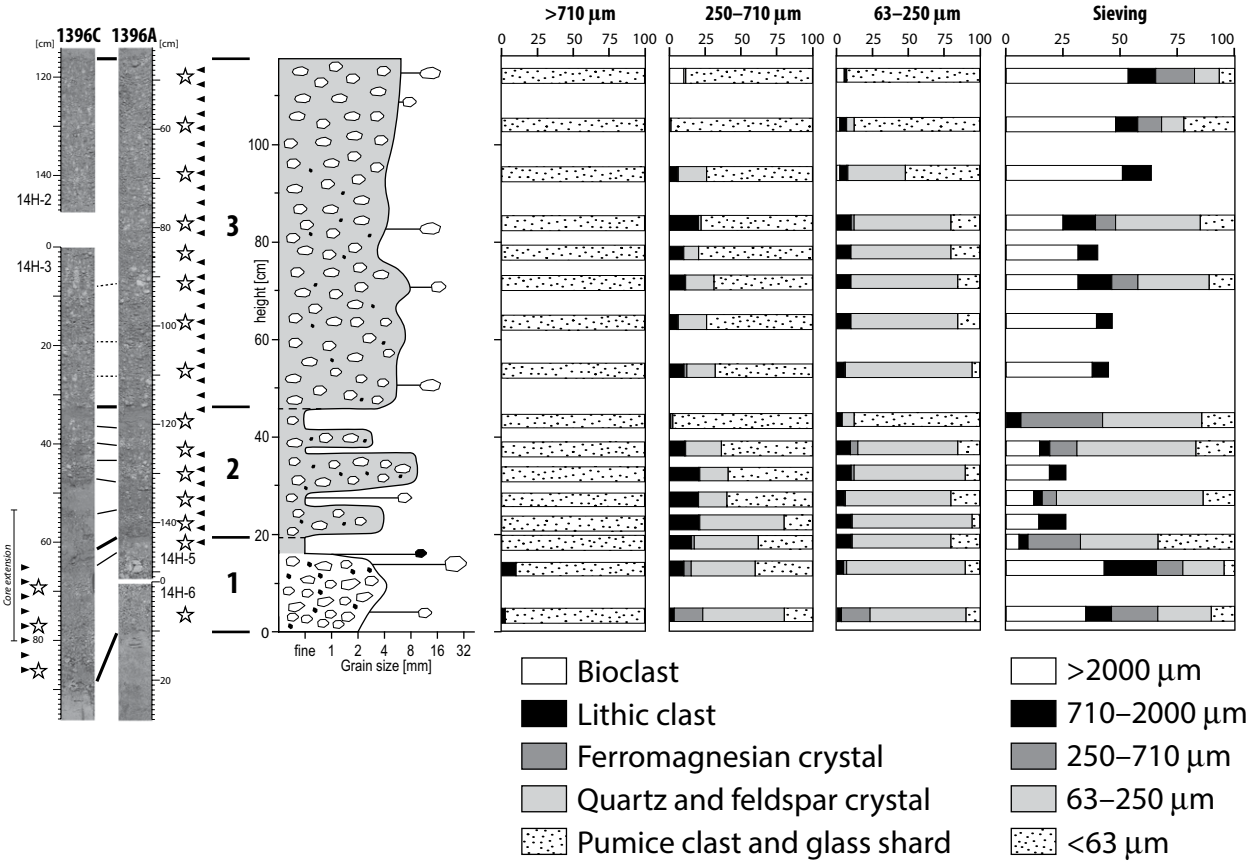

Figure 2. Componentry and sieving of pumice lapilli at Site U1396. (Left) Photos of stratified pumice lapilli-ash in cores U1396C and U1396A. (Center left) Stratigraphic log from visual observations and subunit boundaries. (Center right) Componentry for three grain-size classes, with coarse (>710 µm) particles, medium to coarse (250–710 µm) particles, and very fine to fine (63–250 µm) particles. (Right) Dry sieving data with bins corresponding to componentry analyses; see Figure 5 for complete grain-size analysis. Proportion (%) of grains was estimated from binocular observations. Stars indicate bulk samples taken for componentry and grain-size analyses (this figure and Fig. 5); black triangles indicate pumice clasts taken for flotation experiments.

unit attest to the perfect preservation of the unit and absence of coring disturbances (cf. Jutzeler et al., 2014d, 2016). A few scattered pumice clasts occur in the lower few centimeters of the overlying unit of hemipelagic mud. The stratified pumice lapilli-ash unit displays exactly the same stratigraphy at the two holes, located 40 m apart. However, during onboard splitting of the core, slurries and clast reorganization were observed in the highly porous, fluid-saturated base of U1396C-14H3, resulting in local modification of pumice and lithic grading and minor core extension over 20 cm (cf. Jutzeler et al., 2014d). For this reason, facies description is solely based on the undisturbed core U1396A-14H.

The stratified pumice lapilli-ash is fully unconsolidated and chiefly consists of unaltered pumice clasts (white, highly vesicular, pristine glass) and crystal fragments (mostly feldspar and quartz, with a few ferromagnesian minerals), minor lithic clasts (chiefly nonvesicular/low-vesicularity andesite), and rare foraminifera tests (Fig. 2). The deposit is 1.2 m thick, which makes it by far the thickest undisturbed volcaniclastic unit cored at Site U1396. For comparison, the ~171 volcaniclastic intervals in Site U1396A have a modal thickness of 2 cm, with 84% of the volcaniclastic intervals being <8 cm thick; the thickest of six undisturbed intervals is 42 cm thick (Expedition 340 Scientists, 2012; Jutzeler et al., 2016). Tiny oxidized authigenic pyrite crystals (with framboidal texture) that preferentially grew on fine to extremely fine ash particles give a slight pink hue to the unit and occur in a few other pumice-rich units at this site.

The color, type of components, and modal grain size of the volcanic clasts in the stratified pumice lapilli-ash unit are the same throughout its entire thickness. However, the abundance in components and amplitudes of grain-size modes vary in the stratigraphy over subtle to sharp stratifications. Foraminifera tests occur only in the upper boundary of the unit and do not show reworking of species older than 4.3 Ma (Expedition 340 Scientists, 2012). Here, we subdivide the stratified pumice lapilli-ash unit into three main subunits, described from the base up, using core photos and 18 samples (Figs. 2 and 3).

(1) Subunit 1 is 18 cm thick, subdivided into a 15 cm base that is clast supported and very poor in extremely fine (<63 µm) ash particles, and it is gradationally capped by 3 cm of extremely fine ash particles at its top. The base of the subunit is relatively well sorted, mostly composed of subrounded pumice clasts and crystal fragments, and minor lithic clasts (Fig. 4). It is reversely graded in size of pumice and lithic grains, and in abundance of lithic clasts. The largest pumice (30 mm) and lithic (10 mm) clasts of the entire stratified pumice lapilli-ash unit occur in the upper part of this subunit. The medium- to fine-grained ash mode includes crystal fragments (including abundant ferromagnesians at the base), glass shards, and lithic clasts. The extremely fine-grained ash top is chiefly made of crystal fragments, including relatively abundant ferromagnesian minerals.

(2) Subunit 2 is 26 cm thick and consists of a succession of three pumice-rich beds, each of them capped by fine ash beds slightly varying in color and grain size; all contacts are gradational. The bodies of the three pumice-rich beds are nongraded, although the presence of their respective caps produces normal grading in grain size and abundance of pumice clasts for each bedset. The coarse ash and lapilli (>710 µm) are entirely made of pumice clasts, whereas crystal fragments, glass shards, and lithic clasts are present in the medium to coarse ash (250–710 µm); the very fine to fine ash (63–250 µm) is chiefly composed of crystal fragments. The crystal fragments decrease in abundance up section, with corresponding increases in small pumice clasts and glass shards. This cryptic grading shows that the matrix is density graded. Up to 20% of <250 µm particles are lithic clasts,

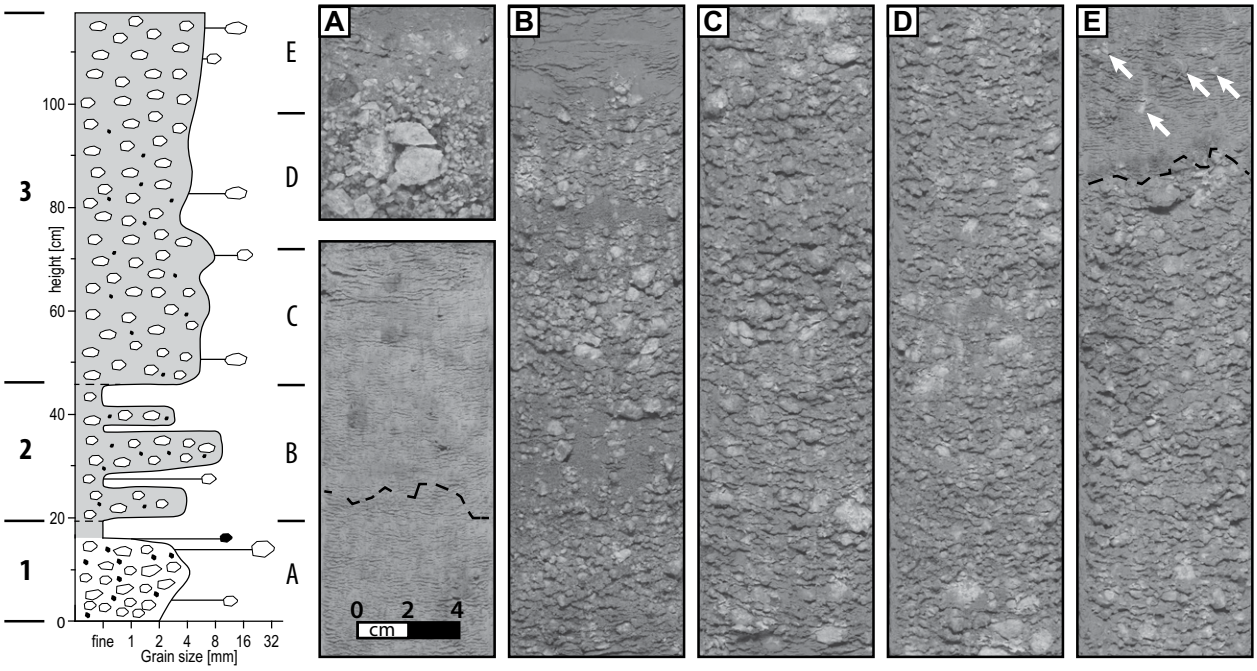

Figure 3. Close-up photographs covering the entire length of the stratified pumice lapilli-ash. (A) Subunit 1 shows sharp contact (dashed line) with underlying hemipelagic mud, slight reverse grading in lithic clasts upward, and fine-grained top. A coarse pumice clast was broken into three pieces during core splitting. (B) Subunit 2, showing three intervals with fine top, all in fully gradational contact. The uppermost part is extremely fine grained. (C) Base of subunit 3, with weak gradational stratifications in size of pumice clasts. (D and E) Middle and top of subunit 3, respectively, with same facies in middle part, and overlying hemipelagic mud (dash line for contact) with dispersed pumice clasts (white arrows).

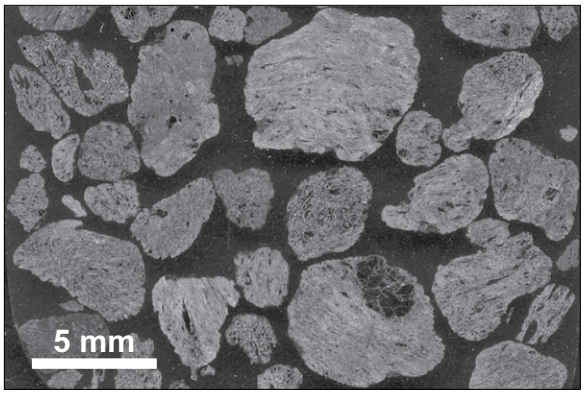

Figure 4. Polished thin section scan of subrounded pumice clasts from U1396A-14H5, 134–136 cm.

which is the highest concentration throughout the entire unit.

(3) Subunit 3 is 71 cm thick; it is the thickest and least stratified of the three subunits, and it does not have a fine-grained top. The subunit consists of a single bed that has weak lamination defined by subtle variations in abundance and size of pumice lapilli (2–20 mm). As in the other subunits, these variations are perfectly matched in the two holes separated laterally by 40 m. Coarse-ash and lapilli (>710 μm) particles exclusively consist of pumice clasts, whereas medium to coarse ash (250–710 μm) particles are chiefly glass shards (>70%) with minor crystal fragments and lithic clasts. Very fine to fine ash (63–250 μm) particles are chiefly crystal fragments that strongly decrease in abundance upward (90%–1%), with corresponding increases in small pumice clasts and glass shards (15%–93%), producing a density-graded matrix as in subunit 2. Medium-ash lithic clasts are absent at the top, and medium- and fine-ash–sized foraminifera tests (up to 5%) occur over the uppermost 15 cm.

Combined grain-size distributions obtained by sieving and laser particle analysis (see Methods) describe the full grain-size distribution (1 μm to 30 mm) for 18 samples (Fig. 5). The grain-size distribution in the stratified pumice lapilli-ash unit reveals five main modes, three of which occur in virtually all samples, although the amplitude of each mode varies considerably among samples. The modes are: pumice clasts at –3 phi (8 mm); pumice clasts at –1.5 phi (2.8 mm); lithic clasts at –0.5 phi (1.4 mm); crystal fragments and glass shards with minor lithic clasts at 2.25 phi (210 μm); and undifferentiated particles at 5–6 phi (3–15 μm).

The stratified pumice lapilli-ash has a very good internal organization by size of grains with respect to the entire unit and within each subunit. The coarse base of subunit 1 mostly has grains in two modes (–3 and –1.5 phi), with a moderate mode at 2.25 phi and a very weak mode at 5–6 phi. In contrast, its top has the opposite behavior, with a prominent mode of fine to very fine-grained ash and weak coarse-grained ash modes. Through subunits 2 and 3, a nearly perfect density grading is achieved with progressive increase in abundance of light (–1.5 phi) pumice clasts and respective decrease in denser crystal fragments and glass shards (2.25 phi) up the stratigraphic section. The extremely fine-grained ash (5–6 phi) increases in proportion up section. This density grading is shown for each of the three levels in the core, and it reflects the transition between subunits 2 and 3, and the uppermost part of subunit 3.

Minor foraminifera tests occur in the uppermost 25 cm of the unit and increase slightly in abundance and size upward (Fig. 2). The presence of small stalactite-like domains in the uppermost 5 cm probably represents postdepositional infill of hemipelagic mud in the porous top of the stratified pumice lapilli-ash.

Pumice Clasts

Given their abundance in this unit, pumice clasts require detailed assessment. Pumice clasts contain a few percent of 0.3–3 mm plagioclase phenocrysts. Lapilli and coarse ash-sized pumice clasts are subrounded, and vesicles are not discernible with the naked eye. Pumice porosity, calculated following Archimedes' principle (see Methods), ranges from 65% to 85%, with a median pumice porosity of 73.7% (Fig. 6; 97 clasts; distribution mean at 73.9%), which matches the common vesicularity of highly evolved pyroclastic pumice (Klug and Cashman, 1996). Assuming a bulk dense rock (i.e., glass and crystal) density of 2400 kg/m^3, the dry bulk density of the vesicular pumice would range 360–840 kg/m^3 (median at 632 kg/m^3), and the mean fully waterlogged pumice density would be 1360 kg/m^3. Image analysis and functional stereology (Jutzeler et al., 2012, 2015b) applied to scanning electron microscope (SEM) images of four representative pumice clasts, and multiple microtomography images (see Methods) reveal three types of pumice vesicularity (Figs. 7 and 8) and a similar range of porosity as that calculated by Archimedes' principle (Fig. 9). The three types of pumice have similar modal vesicle size, ranging from 2 to 4 μm and from 28 to 56 μm, but they differ strongly in the amplitude of each mode. The most abundant type of pumice (termed type 1) includes coarse, ~1-mm-long tubular vesicles surrounded by a small-sized vesicle population (Figs. 7A, 7C, and 7D). Type 2 pumice is the equivalent of type 1 pumice, although the vesicles are not stretched (Figs. 7B, 7E, and 7F). Pockets with numerous, very small vesicles, resembling the main pattern of vesicularity in type 3 pumice, occur in some places (Figs. 7G and 7H). The third type of pumice (type 3) is rare and is mainly characterized by extremely small vesicles (down to 0.5 μm) and thick bubble walls (Fig. 8). Apart from a weak increase in porosity upward in subunit 1, the pumice porosity and clast circularity (shape factor; Dellino et al., 2005) do not change systematically through the stratigraphy (Fig. 9).

Thirteen samples imaged by microtomography show stretched vesicles in type 1 pumice, in contrast to spherical vesicles in type 2 pumice (Fig. 7). Microtomography of entire clasts shows the pumice to lack any impurities (e.g., hemipelagic mud, residual water) that could modify its buoyancy during the flotation experiments.

GEOCHEMISTRY

EPMA analyses of glass in 15 pumice clasts (1–3 analyses per clast) of varied vesicularity and selected across all subunits (Fig. 10; supplemental material [see footnote 1]) show that glass is pristine, nonaltered, and of homogeneous rhyolitic composition (75.1–78.5 wt% SiO_2; 5.2–6.5 wt% $Na_2O + K_2O$). Bulk pumice composition is also rhyolitic (Fig. 10; supplemental material [see footnote 1]). In addition to textural evidence showing similar color, crystal content, and vesicle texture for all pumice clasts (Fig. 3), geochemical homogeneity strongly suggests that pumice clasts are juvenile and from the same eruption. The geochemical composition of the unit is much more evolved than that of most analyzed andesitic rocks in the Lesser Antilles arc, making it difficult to pinpoint the provenance of the stratified pumice lapilli-ash unit using bulk rock geochemistry or glass analyses (Fig. 10). Pb isotopic analyses (Fig. 11; supplemental material [see footnote 1]) of pumice clasts from the base of subunit 1 (U1396C-14H3, 85–87 cm) and from the middle of subunit 3 (U1396A-14H5, 68–70 cm), of fines from subunit 2 (U1396A-14H5, 138 cm), and of lithic clasts from subunit 1 (U1396C-14H3,

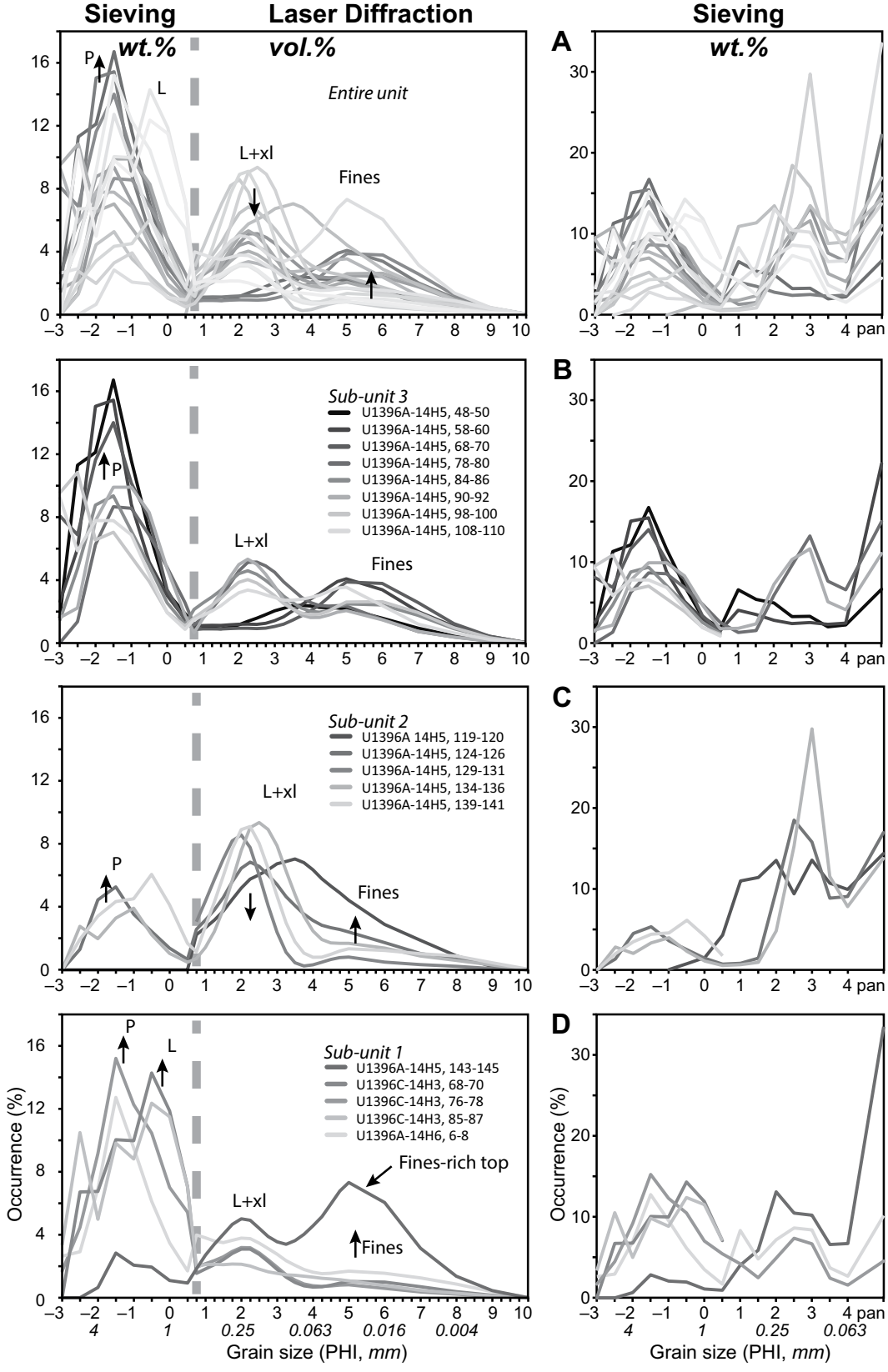

Figure 5. Granulometry and grain-size distribution of the pumice-lapilli-ash. (Left) Sieving data (coarse grained) combined with laser diffraction data (fine grained). Line darkness increases up stratigraphy. Lithic clasts (L) and crystal fragments (xl) overall decrease in abundance up stratigraphy, whereas pumice clasts (P) and extremely fine particles increase in abundance. Lithic clasts in subunit 1 show an abnormally high peak at –0.5 phi, due to their high density compared to pumice clasts. Sieving data (–3–1 phi) are in weight% (wt%), whereas laser diffraction data (0.75–10 phi) are in volume% (vol%); both sets of measurements are normalized to 100% according to their respective bulk wt% at the 0.75 phi cutoff (see text). (Right) Sieving data down to 4 phi. The grading pattern is very similar to laser diffraction data, although clast density modifies some trends. (A) Entire stratigraphy; (B) subunit 3; (C) subunit 2; (D) subunit 1.

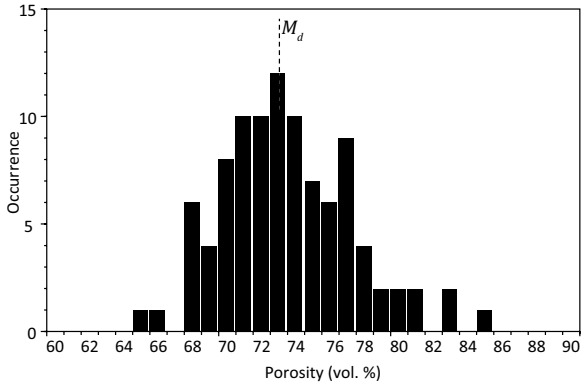

Figure 6. Porosity histogram for pumice clasts of stratified pumice lapilli-ash used in experiments. Median, M_d. Pumice clasts were 2.3–22 mm length.

85–87 cm) match those of material from the Soufrière Hills volcanic center on Montserrat (36 km to the northeast) defined by Cassidy et al. (2012). Age correction related to decrease in radiogenic Pb isotopes could not be calculated for the pumice clast samples analyzed by XRF due to the low concentration of uranium (<2 ppm), which was below our instrument's detection limit (see footnote 1).

SUBAQUEOUS SEDIMENTATION

Settling Column Experiment

Particle settling in water is strongly influenced by the density and viscosity of water. Clasts are sorted by hydraulic effects, which are a function of their drag, corresponding to clast size, density, and shape (Manville et al., 2002; Burgisser and Gardner, 2006; Jutzeler et al., 2015b). Using a settling column, the hydraulic equivalence of natural samples containing different types of clasts with varying particle densities (e.g., pumice vs. crystals) can be analyzed to aid in inferences about sedimentation processes.

Settling experiments were carried out with cold clasts (ambient temperature), where the pumice clasts had been submerged for 1 wk prior to the experiment. Settling experiments show separation into three main modes of deposition (Fig. 12) that matched the grain-size distribution. Coarse (>1 mm) pumice clasts were the fastest to sink, followed by finer particles (small pumice, lithic, crystal), down to extremely fine ash particles, which showed a truncated mode due to the experiment setup (see Methods). For a given sample, grain density is the main variable connecting the settling size distribution with the grain-size distribution. Grain density can be calculated from the settling data. Here, pumice clasts have a mean partly waterlogged density of 1180 kg/m^3, which corresponds to 75% water-filled and 25% gas-filled vesicles for a mean pumice porosity of 74% (i.e., a 100% waterlogged pumice would be 1364 kg/m^3). This value is consistent with the pumice clasts having been immersed in water for only a week, which is insufficient for water to reach small air-filled pores in a cold pumice at very low hydrostatic pressure (Manville et al., 1998; White et al., 2001). During natural settling in the ocean, any gas present in the vesicle would both dissolve and compress with increasing hydrostatic pressure during descent. The fine to very fine ash mode is broad, due to mixed componentry (pumice, lithic, and crystal). Visually, small lithic and pumice clasts appear to have settled first, followed by crystals, and then a mixture of unidentified particles. The density of the fine to very fine ash mode is ~2000 kg/m^3, and this is consistent with the bulk density of mixed pumice and dense clasts. The experimental first arrival of crystals matches their theoretical density (2650 and 2690 kg/m^3 for quartz and plagioclase andesine, respectively). Settling speeds calculated during our experiments ranged from 0.075 to 0.078 m/s for 5–15-mm-long pumice clasts, and 0.006–0.015 m/s for medium-ash–sized particles, and these values match data from Cashman and Fiske (1991).

Sizing of Pumice Clasts by Hydraulic Sorting

In water, hydraulic sorting of clasts is mainly a function of their size and density (Cashman and Fiske, 1991; Jutzeler et al., 2014b, 2015b). To assess the grading of porous clasts in a subaqueous deposit, we needed a single value that described the hydraulic size of the clasts. The "hydraulic grain size" corresponds to the right-hand part of Equation 7 in Jutzeler et al. (2015b):

$$\left(\frac{\rho_{\text{Pumice}} - \rho_{\text{Fluid}}}{\rho_{\text{Fluid}}}\right) d_{\text{Pumice}} \quad \text{for settling clasts with Re}>10^3, \qquad (1)$$

where ρ_{Pumice} is the wet clast bulk density, ρ_{Fluid} is the fluid density, and d_{Pumice} is the clast size. This equation is restricted to transport with absence of shear or rolling on the substrate. This hydraulic grain size for settling of clasts can be used for clasts with Re >10^3, which corresponds to pumice clasts >5–8 mm or dense clasts >3 mm (Jutzeler et al., 2015b), consistent with the pumice clasts recovered from Site U1396. Therefore, knowing the density and size of a pumice clast, the sedimentologically relevant grading of a submarine deposit can be assessed.

In Figure 9, we calculated the hydraulic grain size using porosity and size of each pumice clast. The hydraulic grain size slightly increases (i.e., reverse grading) upward through subunits 1 and 2. In subunit 3, there is a more apparent decreasing trend in hydraulic grain size, corresponding to a normal grading of pumice clasts. There is little variation in pumice porosity (vesicularity, density), so overall, these grading trends mimic the grain-size trends for the selected clasts.

Hydraulic Equivalence

Using settling column and hydraulic grain-size values, it is possible to quantify the hydraulic equivalence of the stratified pumice lapilli-ash. Hydraulic equivalence of settled clasts with mixed densities can be assessed using Equation 11 of Jutzeler et al. (2015b), which uses a hydraulic sorting ratio, equivalent to dividing the hydraulic grain size of pumice clasts (Eq. 1 in this study) by the hydraulic grain size of lithic clasts. Using values from the settling column experiments, pumice clasts (–2 phi) are not hydraulically equivalent to any of the other modes of particles. The first medium-sized particles to settle (1 phi) have a hydraulic sorting ratio of 1.5 in relation to pumice clasts, whereas the mode of fine particles (2 phi) gives a hydraulic sorting ratio of 2.5 in relation to pumice clasts. These hydraulic sorting ratios >1 show that the pumice clasts are too coarse to have been in hydraulic equivalence with finer-grained particles in the same layer (Jutzeler et al., 2015b). The mismatch in hydraulic grain size indicates that the stratified pumice lapilli-ash was not deposited during a single event of subaqueous sedimentation that had efficient hydraulic sorting.

FLOTATION EXPERIMENTS

Simple flotation experiments can re-create conditions of pumice waterlogging, allowing inferences to be made about the residence time at the water surface, and transport and sedimentation behaviors associated with submarine pumice-rich deposits. Here, we carried out experiments at ambient (20 °C) and close to magmatic (600 °C) temperatures to re-create end-member conditions of interaction with seawater.

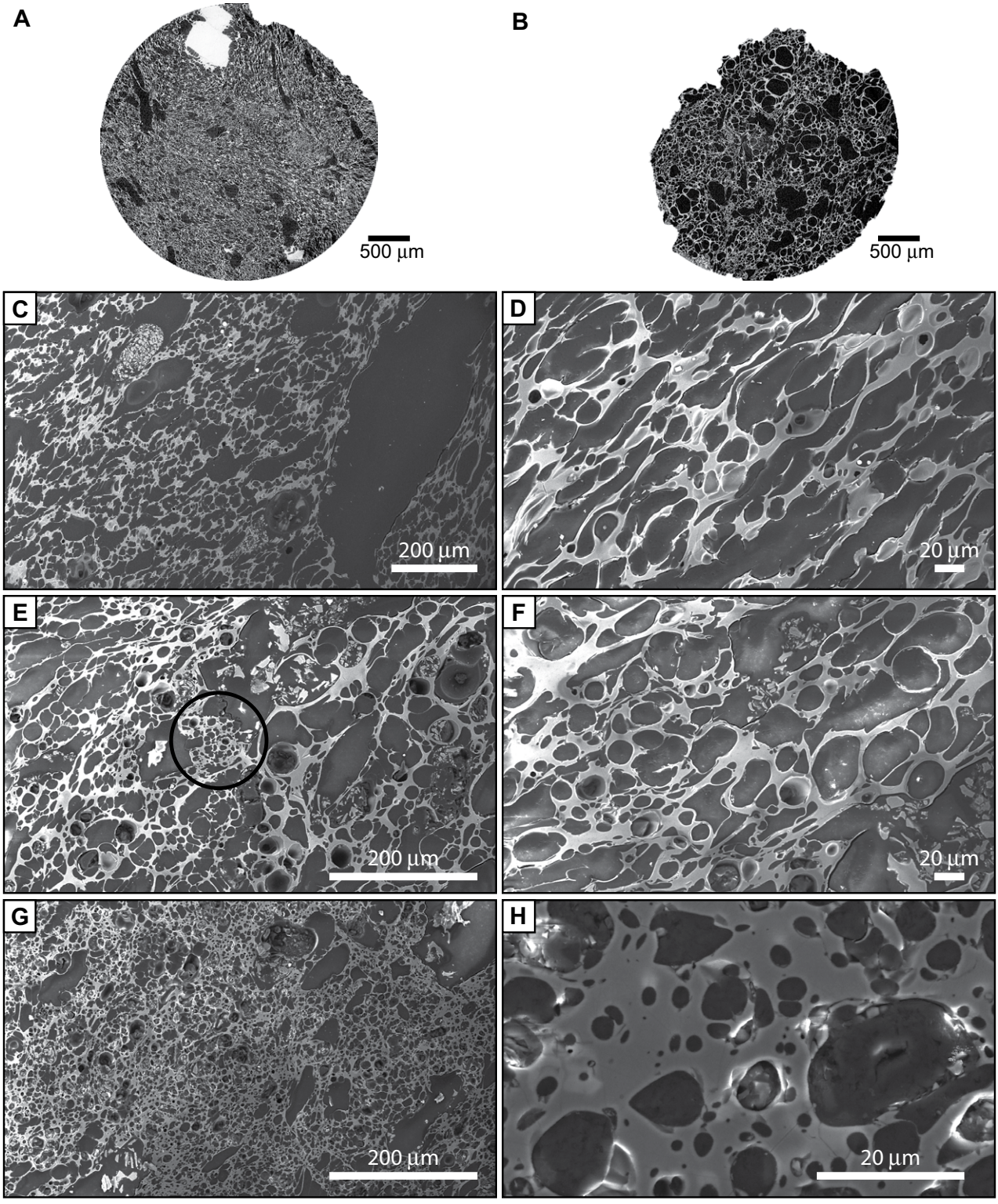

Figure 7. Images of three types of pumice vesicularity. Pumice type 1 is the stretched equivalent of most abundant pumice type 2. Pumice type 3 is very finely vesicular. (A) Microtomography image of type 1 pumice at U1396A-14H5, 54 cm. (B) Microtomography image of type 2 pumice at U1396A-14H5, 87 cm. (C) Scanning electron microscope (SEM) image of pumice P-a (type 1) at U1396A-14H5, 48 cm; pumice has elongated, large-size tubes. (D) Close-up of C. (E) SEM image of pumice P-b (type 2) at U1396A-14H5, 48 cm, with chiefly round vesicles. Pockets (black circle) of type 3 pumice occur. (F) Close-up of E. (G) SEM image of pumice P-8 (type 3) in at U1396A-14H6, 6 cm; pumice has thick vesicle walls. (H) Close-up of G, showing extremely small vesicles and thick bubble walls. See Figure 8 for volumetric vesicle distribution of the pumice clasts P-a, P-b, and P-8.

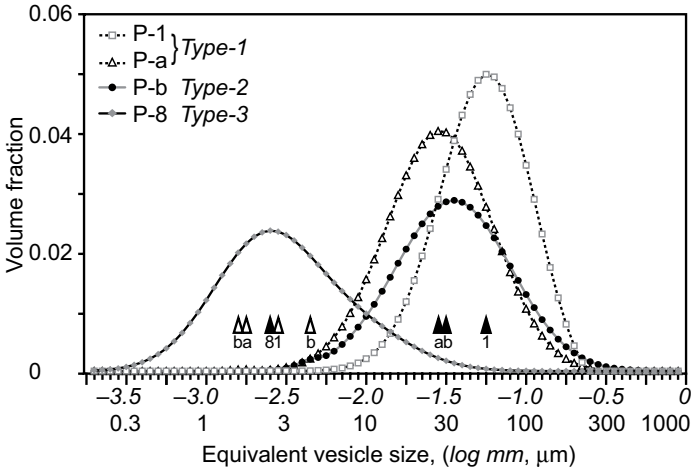

Figure 8. Vesicle number density of four pumice clasts. P-a and P-b have same vesicularity, although P-a is stretched. P-8 has large amount of extremely small vesicles (down to 0.5 μm diameter). All types of pumice share similar modes ranging 2–4 μm and 28–56 μm, although the fine mode seems to not be present in P-1. Pumice P-a is type 1 at U1396A-14H5, 48 cm; pumice P-b is type 2 at U1396A-14H5, 48 cm; pumice P-1 is type 2 at U1396A-14H6, 6 cm; and pumice P-8 is type 3 at U1396A-14H6, 6 cm. Triangles refer to primary (filled) and secondary (hollow) modes for each vesicle population and the adjacent number or letter refers to sample label. See Figure 7 for selected photos of vesicle textures of the pumice clasts P-a, P-b, and P-8.

Background

The vesicles in pumice fragments, in an intricate but mostly connected network (Klug and Cashman, 1996), make them, when dry, buoyant in water for some time but ultimately prone to waterlogging. Flotation experiments and theoretical work have been conducted to study the rate of waterlogging (i.e., rate of water infiltration into open pores) when plunged into water. Rate and efficiency of pumice waterlogging depend strongly on the physical properties of the pumice clast (density, permeability, size) and on its temperature at first contact with water (Whitham and Sparks, 1986; Manville et al., 1998, 2002; White et al., 2001; Risso et al., 2002; Dufek et al., 2007).

At room temperature, the narrow and often tortuous connected vesicle network in pumice will progressively fill with water because of capillary action, which includes the combined forces of interfacial tension and hydrostatic pressure of the water outside the pumice (Whitham and Sparks, 1986; White et al., 2001; Vella and Huppert, 2007), implying a relationship between clast volume and flotation time. Risso et al. (2002) found a better relationship with the clast's shortest (i.e., *c*-axis) diameter, supported by the reasonable assumption that the widest cross section of the clast will lie parallel to the water surface while it floats, thus maximizing the clast's wetting surface. Cold pumice waterlogging times range from minutes to years (Whitham and Sparks, 1986; Manville et al., 1998; White et al., 2001; Risso et al., 2002; Jutzeler et al., 2014a).

A very different type of waterlogging occurs at hot temperatures (>300 °C), where pumice clasts can sink in a matter of seconds. Experiments show that air or residual magmatic steam present in vesicles quickly cools and reduces in volume. Steam of magmatic origin or from

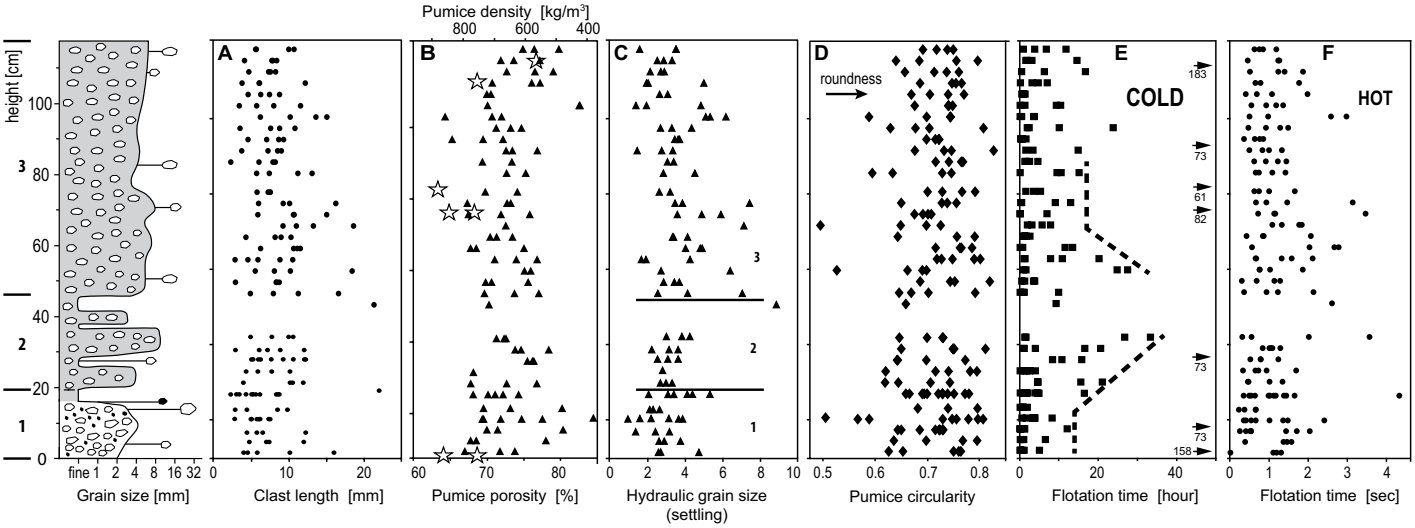

Figure 9. Grain size, porosity, hydraulic grain size, clast shape, and results from flotation experiments through stratigraphy. Selected pumice clasts are mostly >5 mm; each interval contains one small pumice clast, which can be 2–5 mm. (A) Length of selected pumice clasts. (B) Porosity of selected pumice clasts, calculated by Archimedes' law (triangles) and image analysis from microtomography images (stars). Density was calculated from values of porosity. Data show no correlation with stratigraphy. (C) Hydraulic grain size (see text) for selected pumice clasts, showing weak increase through subunits 1 and 2, and weak decrease through subunit 3. Dashed lines show main linear trends. (D) Clast shape (circularity). (E) Cold flotation experiment data, showing relatively fast waterlogging; arrows show time for nonplotted outliers. Dashed lines show broad increase and decrease in the threshold of flotation time. (F) Hot flotation experiment data, showing fast waterlogging of all clasts and no stratigraphic correlation.

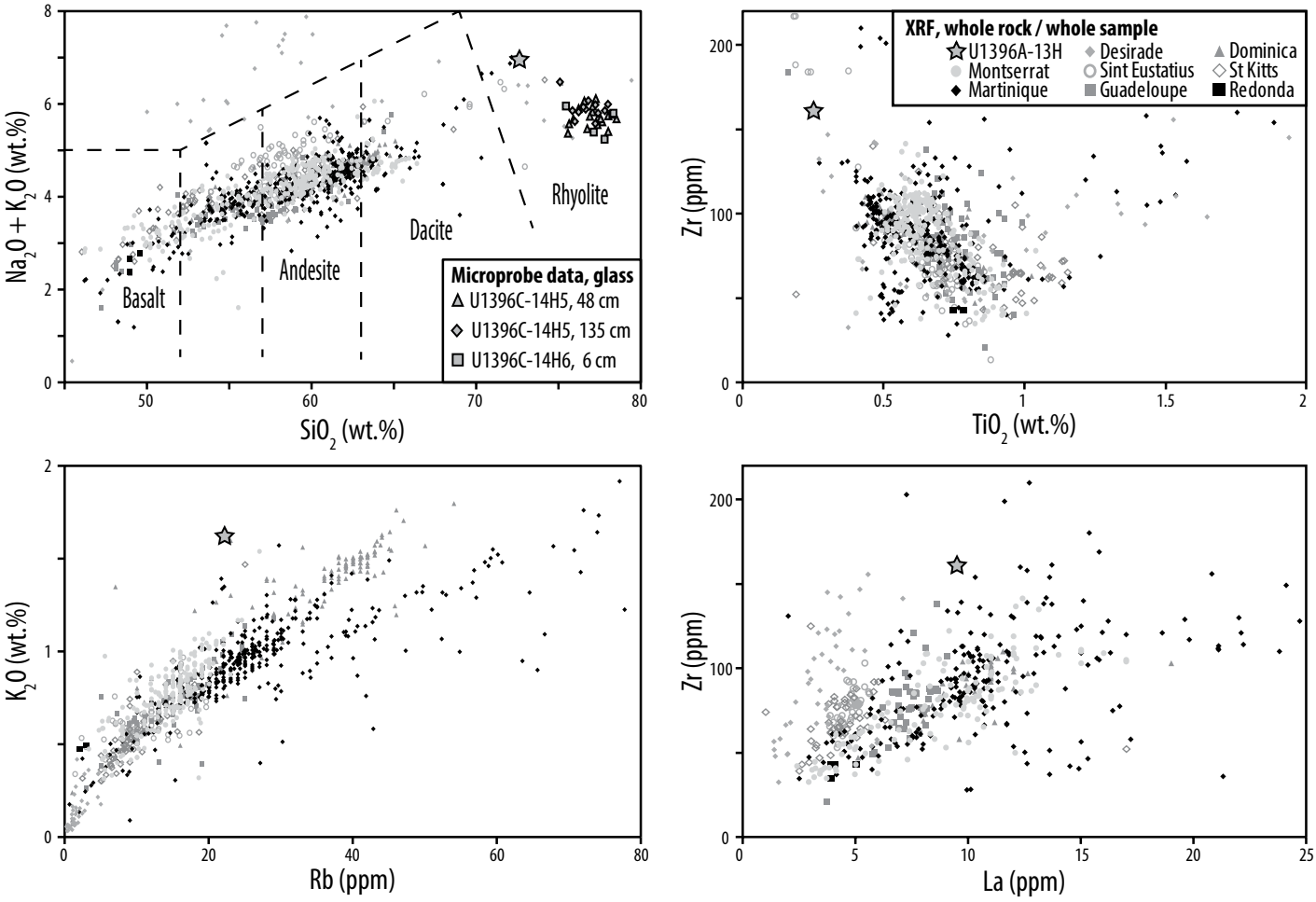

Figure 10. Bulk rock (X-ray fluorescence [XRF]) and glass (electron probe microanalyzer) geochemistry in the stratified pumice lapilli-ash, compared with published data (GEOROC) from nearby islands. Studied unit is more evolved than most rocks in the Lesser Antilles, and data do not match a particular compositional trend.

boiling external water condenses, leading to external water being drawn into the vesicle network (Whitham and Sparks, 1986; Kato, 1987; Dufek et al., 2007; Allen et al., 2008). The rate and efficiency of pumice waterlogging have been proposed to be proportional to the clast's mass (Dufek et al., 2007) and temperature (Whitham and Sparks, 1986; Campbell et al., 1987).

At medium-hot temperatures (150–300 °C), nonlinear variations in the rate of pumice waterlogging occur due to variations in the boiling style at the surface of the hot clasts at contact, passing from nucleate boiling to film boiling at high temperatures (Mills, 1984; Whitham and Sparks, 1986; Campbell et al., 1987). Such variations might influence the rate of evaporation and thus rate of waterlogging, but they were not tested in our experiments. To avoid complications arising from the style of boiling, hot experiments were conducted with particle temperatures of 600 °C, a reasonable temperature for fresh rhyolitic pyroclasts and one at which film boiling is ubiquitous.

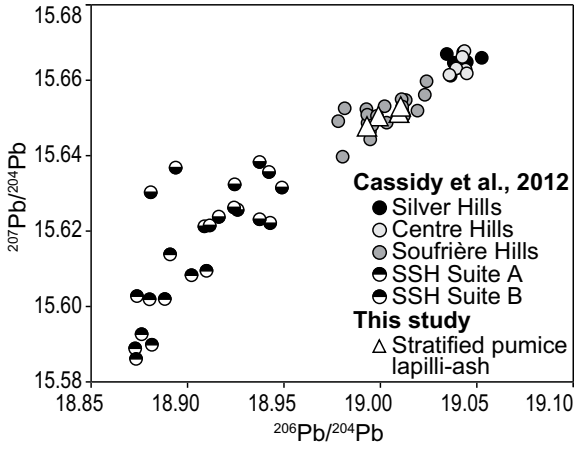

Figure 11. Pb isotope data of stratified pumice lapilli-ash compared with rocks from Montserrat (Cassidy et al. 2012). Pumice, lithic, and medium-sized particles from the stratified pumice lapilli-ash perfectly match the composition from Soufrière Hills from Cassidy et al. (2012; medium gray). SSH—South Soufrière Hills.

Results from Flotation Experiments

Cold Experiments

Four to five pumice clasts with longest (*a*-axis) diameter of 2.3–22 mm were randomly picked every 3 cm (where occurring) up section through the stratified pumice lapilli-ash. After sample cleaning and drying (see Methods), the

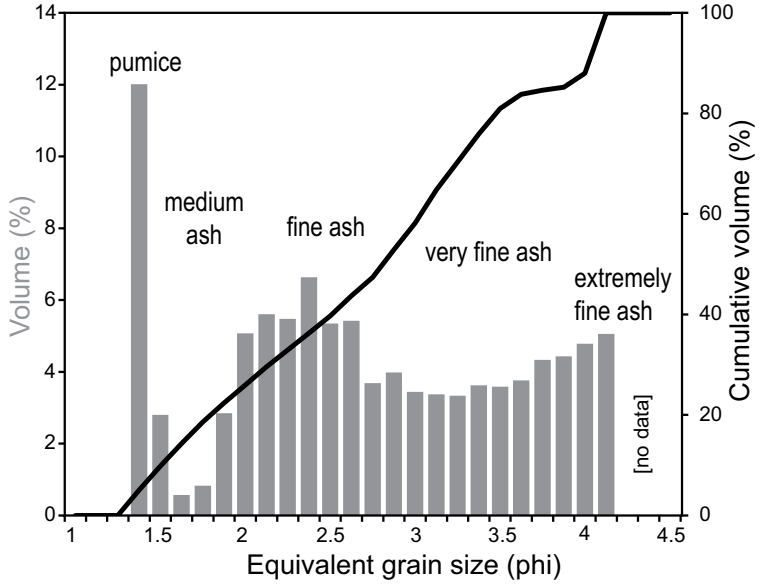

Figure 12. Settling column experiment data. Average of four very similar data sets taken through the stratigraphy, including a bulk sample, "pumice," "medium and fine," and "very fine" runs. For representation purpose, calculated settling equivalence is with spherical quartz grains of 2650 kg/m^3. Data >4 phi were not recorded.

pumice clasts were dropped onto a water-filled container and left to float until they sank. Once clasts reached the water surface, we observed weak bubbling from some, and these commonly rotated in the last stage of flotation. Cold flotation data (20 °C) for these –1.2 to –4.5 phi particles show that 50% of pumice clasts sank within 2 h, 84% within 12 h, and 94% within 24 h (Fig. 9); a few outliers floated much longer; these occurred at all levels of the deposit. In subunit 2 and at the base of subunit 3, selected pumice clasts took longer to sink than the average time (Fig. 9). The floating time of the studied pumice clasts correlates well with their porosity (Fig. 13), but not with their size (diameter, volume), mass, shape factor, or aspect ratio. Moreover, there is no relationship between flotation time of the cold pumice clasts and their stratigraphic position, implying the deposit is not simply graded by pumice saturation (see White et al., 2001).

For reference, cold experiments were conducted on additional pumice clasts sampled as isolated clasts within hemipelagic mud (pumice dropstones), or from very thin intervals thought to be deposited from pumice rafts. These clasts were sampled much further up section, from core sections U1396A-8H2, 8H3, 9H4, and 9H5, and are thought to originate from Montserrat or Guadeloupe islands. These clasts show very similar flotation time to clasts in the stratified pumice lapilli-ash (Fig. 14).

Hot Experiments

Hot (600 °C) experiments were conducted on the same pumice clasts used for the cold experiments. In contrast to the cold experiments, the pumice clasts floated only for a few seconds (0.23–4.32 s; Fig. 9), during which there was vigorous bubbling, steaming, and hissing. High-speed camera images clearly showed numerous underwater steam bubbles evacuating the clasts as soon as they touched water, with bubbling subsiding in intensity after the first second of immersion. As in the cold experiments, some clasts rotated in their last moment of floating. The flotation time from hot experiments showed that longer-floating clasts were not taken from the top of the stratified pumice lapilli-ash (Fig. 9); thus, pumice clasts did not show a simple trend of saturation grading (see White et al., 2001).

Comparison with Published Data

Overall, the cold pumice clasts of this study sank at rates orders of magnitude higher than those of cold pumice clasts studied by other workers (Fig. 14; Whitham and Sparks, 1986; White et al., 2001; Risso et al., 2002). For cold pumice clasts, our data do not follow the apparent linear trend between flotation time and pumice size (volume and diameter) shown by the Taupo pumice. The coarseness of the studied Minoan (Santorini) and Protector Shoal pumice clasts makes comparison difficult. Pumice clasts selected from the other core from U1396 also showed similarly brief cold flotation times.

Flotation time of the hot pumice clasts from this study is correlated with their size (diameter and volume) and mass, but not with their porosity (in contrast to cold experiments), shape, or aspect ratio (Fig. 13). Our data set shows a longer sinking time than for the hot Medicine

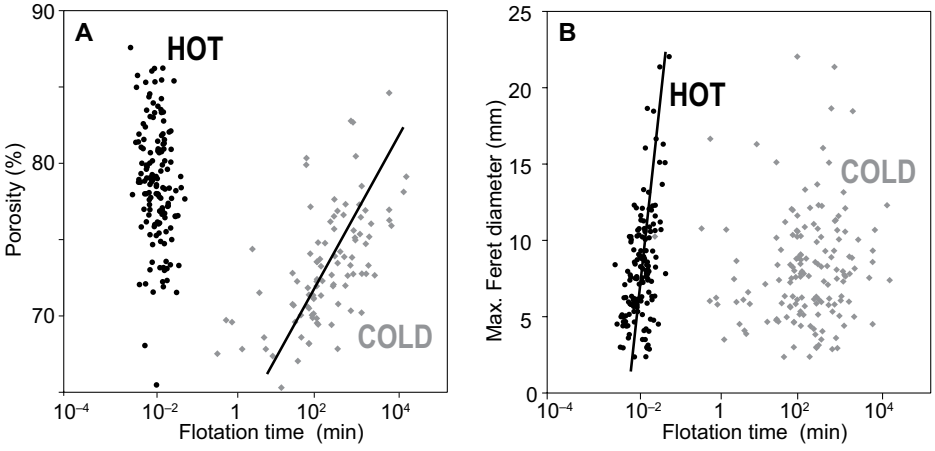

Figure 13. Flotation time for cold and hot experiments. Cold experiment data (gray diamonds) correlate with clast porosity (A), whereas hot experiment data (black dots) correlate with maximum grain length (B).

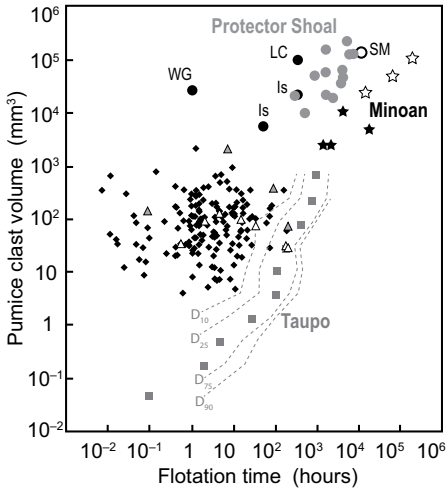

Figure 14. Flotation time of cold pumice from this study compared with published literature. The pumice from the studied unit (black diamonds) sank much faster than ~90% of the Taupo pumice clasts and did not follow the same rate of waterlogging with clast volume. Pumice lapilli from U1396A-8H2, 104 cm (open gray triangles), and other pumice clasts from U1396A-8H2, 8H3, 9H4 and 9H5 (filled gray triangles; see text), interpreted as rafted pumice clasts, share similarities with the pumice from the stratified pumice lapilli-ash and with the Taupo pumice. Symbols: gray squares and dashed gray percentiles lines—Taupo Plinian (A.D. 232 eruption; New Zealand; White et al., 2001; Hogg et al., 2012); gray dots—Protector Shoal (1962 eruption in the Sandwich Islands, sub-Antarctica; Risso et al., 2002); black and open (inferred data) stars—Minoan Plinian (1500 B.C. eruption at Santorini, Greece; Whitham and Sparks, 1986); WG—W-tephra (Guatemala; Whitham and Sparks, 1986); Is—Ischia (San Angelo, Italy; Whitham and Sparks, 1986); LC—Los Chocoyos (Guatemala; Whitham and Sparks, 1986); SM (inferred data)—Santa Maria (Guatemala; Whitham and Sparks, 1986).

Lake samples (Dufek et al., 2007), especially for the smallest clasts; however, both data sets show a good relationship between time to sink and size of the hot pumice clasts (Fig. 15).

DISCUSSION

Origins and Provenance of the Stratified Pumice Lapilli-Ash

A pyroclastic origin for the entire stratified pumice lapilli-ash unit is implied by several features: (1) There is a high abundance of relatively fine-grained (lapilli and ash) rhyolitic pumice clasts mixed with crystal fragments and glass shards; (2) the glass composition of the pumice clasts is homogeneous; (3) crystal-fragment mineralogy is consistent with the pumice's highly evolved glass composition, including trace-element and Pb isotope compositions that show that pumice, lithic fragments, and bulk fines (including crystal fragments) have a common magmatic source (Figs. 9, 10, and 11; supplemental material [see footnote 1]).

The provenance of the stratified pumice lapilli-ash is difficult to determine from major and trace element geochemistry alone (Fig. 10). The overall andesitic Lesser Antilles arc erupts magmas with similar major- and trace-element concentrations from its various volcanic islands (Macdonald et al., 2000). The stratified pumice lapilli-ash is rhyolitic in composition and hence does not lie along the compositional trends of rocks from the nearby islands. Its evolved composition may reflect a rare and unusual magmatic event, probably of large magnitude, which may not have occurred again at Montserrat since 4 Ma.

Pb isotopic ratios of this unit (Fig. 11) match well with those of rocks from the Soufrière Hills volcanic center on Montserrat (36 km to the northeast), which is the closest volcano to Site U1396. No other nearby island has rocks with similar Pb isotopic ratios. This chemical signature, and the spatial location of the unit, strongly suggests that a volcano with a similar magmatic source to Soufrière Hills existed at ca. 4 Ma, potentially at the same site. This changes our understanding of the history of Montserrat, where the oldest on-land rocks currently known are from Silver Hills, on the north part of the island, at 2.6 Ma, and where the current volcanic center at Soufrière Hills is only known to have been active since ca. 170 ka (Harford et al., 2002). On the other hand, a ca. 4 Ma age is relatively young with respect to the earliest inferred submarine magmatism of proto-Montserrat at 20 Ma (Briden et al., 1979). The island currently culminates at ~900 m, but with a total elevation above seafloor of ~2 km, implying a long submarine growth history (Le Friant et al., 2004). It is unlikely that there are unknown submarine volcanic centers near U1396, and no submarine vents have been identified from the multiple seismic data sets (Expedition 340 Scientists, 2012). It would also be anticipated that if U1396 were near a vent, the stratigraphy would be dominated by proximal volcanic deposits (e.g., McPhie et al., 1993). The environment in which the eruption is inferred to have begun is addressed later in this paper.

Transport and Sedimentation Processes

The stratified pumice lapilli-ash unit does not match any previously described lithofacies. It is very thick, laterally continuous, gradationally stratified, very poorly sorted, has a clast-supported base grading into a matrix-supported body, includes abundant subrounded pumice clasts and crystal fragments, and contains lithic clasts throughout the unit's stratigraphy; bioclasts are absent from most of the stratigraphy. None of the hundreds of tephra beds collected in basins surrounding volcanic arcs during the Ocean Drilling Program (ODP)/IODP Expeditions 126, 340, and 350 has shown beds that share these facies characteristics (Taylor et al., 1990; Expedition 340 Scientists, 2012; Expedition 350 Scientists, 2014). To our knowledge, there are also no published descriptions of such a deposit from subaerially exposed uplifted submarine successions (McPhie et al., 1993; Allen and Stewart, 2003; Kano, 2003; McPhie and Allen, 2003; Jutzeler et al., 2014b, 2014c), or

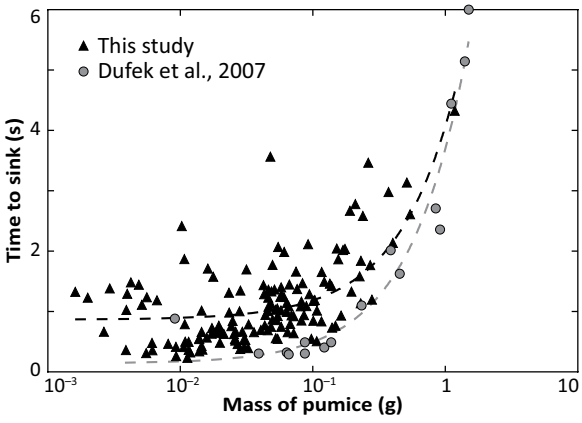

Figure 15. Flotation time of hot pumice vs. pumice mass. Comparison between pumice from this study at 600 °C (triangles) with Medicine Lake pumice at 500 °C (dots; Dufek et al., 2007). Both pumice data sets show correlation with clast size, although Medicine Lake pumice overall sinks faster and is less scattered.

cored deposits of the modern seafloor (Carey and Sigurdsson, 1980; Sparks et al., 1983; Trofimovs et al., 2008, 2012, 2013; Schindlbeck et al., 2013; Cassidy et al., 2014a, 2014b). This suggests that the stratified pumice lapilli-ash resulted from an uncommon transport and depositional process or group of processes. In the next sections, we assess the potential for different marine processes to produce this stratified pumice lapilli-ash facies.

Dilute Ocean Bottom Currents

The perfect match in bed-form stratification in cores located 40 m apart, distinctive pumice texture and geochemistry, relatively poor sorting of the unit, and absence of cross-bedding argue against generation of the deposit by local reworking from dilute bottom currents. For example, tidal- or storm-driven, or bottom currents typically produce more strongly stratified, well-sorted, and laterally heterogeneous deposits, most of which contain low-angle stratification (e.g., Valentine et al., 1984; Ito, 2002; Martín-Chivelet et al., 2008; Stow and Faugères, 2008; Huppertz and Piper, 2010; Jutzeler et al., 2014b).

Turbidity Currents

The present-day bathymetry surrounding Montserrat (Fig. 1) could allow turbidity currents initiated on the apron of Montserrat to reach Site U1396. Overall, the broad facies of the stratified pumice lapilli-ash is comparable to some turbidites, including lateral continuity over tens of meters, unit thickness, stratification, and relatively poor clast sorting (e.g., Talling et al., 2012). The clast-supported subunit 1 could represent deposition from an efficiently fines-elutriated head of a turbidity current, followed by deposition of the poorly sorted mixture from the current body. The stratified subunit 2 is overlain by a more massive subunit 3. Such successions share some resemblance to spaced (or stepped) planar-laminated $T_{B\text{-}3}$ units (Sumner et al., 2012; Talling et al., 2012) of high-density turbidity currents, which grade upward into more massive, slightly density graded T_A units. $T_{B\text{-}3}$ units are thought to be deposited by traction carpets, whereas T_A units are probably formed from parts of a current in which near-bed turbulence is damped, and particle settling is strongly hindered. However, key textures in the stratified pumice lapilli-ash do not match those of deposits from long-runout turbidity currents (Table 1). First, the ~10-cm-thick strata in subunit 2 seem too thick to match a $T_{B\text{-}3}$ facies, which are commonly 5–10 mm thick (Sumner et al., 2012; Talling et al., 2012), although the particle coarseness of the studied unit may have led to formation of thicker-than-usual layers of spaced planar laminae. Moreover, the grading and sorting in the stratified pumice lapilli-ash are extremely poor, with multiple modes ranging over more than 12 phi (a few microns to 6 mm; Fig. 5), which is much worse than the poor sorting documented from conventional turbidites. The multiple separate modes and the noncontinuous grain-size distribution, notably with the near absence of 0.3–1.5 mm clasts, are difficult to produce by a conventional turbidity current, although this might be explained by the grain size produced at the source. Furthermore, there is very poor segregation of pumice clasts from dense ones throughout the entire deposit, and coarse, dense clasts would not be expected to remain in the bulk of a flow while it was simultaneously depositing slower-settling pumice particles (Fig. 3). We note also that extremely fine ash particles (mode at 5–6 phi) occur through most of the deposit. This argues against an origin from an initially hot primary volcaniclastic turbidity current, in which fine-ash particles are commonly elutriated into a suspension plume from which the fines subsequently settle onto the turbidite (White, 2000; Freundt, 2003; Trofimovs et al., 2006, 2008; Cantelli et al., 2008). The abundance of fine-ash particles in the deposit could be attributed to deposition from a cohesive, submarine debris flow, but the laminae and presence of basal clast-supported subunit 1 do not favor this transport mechanism (e.g., Talling et al., 2012). Importantly, intraclasts and bioclasts are absent from most of the deposit, and foraminifera tests only occur within the uppermost part of the unit. Turbidity currents are generally erosive during parts of their

TABLE 1. TRANSPORT PROCESSES CHECK-LIST FOR PUMICE LAPILLI-ASH AT U1396, WITH INITIAL (LEFT) AND FINAL (RIGHT) TRANSPORT PROCESSES

	Initial step			Second step		
Transport types	Pyroclastic flow over water	Fallout over water	Pumice raft	Vertical settling	Seafloor-hugging turbidity current	Dilute bottom current
Distance from coast (Montserrat)	Yes	Yes	Yes	Yes	Yes	Yes
Deposit thickness	Yes	**No**	Yes	Yes	Yes	Yes
Lateral continuity over at least 40 m	Yes	Yes	Yes	Yes, if current deflection	Yes	**No**
Planar bedding only	Yes	Yes	**No**	Yes	Yes	**No**
Sharp basal contact	Yes	Yes	Yes	Yes	Yes	Yes
Stratified deposit	Yes, if multiple pulses	Yes, if multiple pulses	Yes, if multiple pulses	Yes, if multiple pulses	Yes, if multiple pulses	Yes, if multiple pulses
Gradational contacts within deposit	Yes, if multiple pulses	Yes, if multiple pulses	Yes, if multiple pulses	Yes, if multiple pulses	Yes, if multiple pulses	Yes, if multiple pulses
Multiple grain size modes	Yes	Difficult	Yes	Yes	Yes	Yes
Persistent grain size modes	Yes	**No**	Yes	Yes	**No**	**No**
Normal grading	Yes	Yes	**No**	Yes	Yes	Yes
Clast-supported base, matrix-supported top	Yes	Yes	Yes, if raft abrasion	Yes, if multiple pulses	Yes, if multiple pulses	**No**
Basal layer is not exclusively made of dense clasts	Yes	**No**	**No**	Yes	Yes	Yes
Overall very poorly sorted	Yes	**No**	**No**	Yes, if multiple pulses	Yes, if multiple pulses	**No**
Poor hydraulic sorting	Yes, if multiple pulses	Yes, if multiple pulses	Yes, if multiple pulses	Yes, if multiple pulses	Yes, if multiple pulses	**No**
Single type of pumice	Yes	Yes	Yes	Yes	Yes	**No**
Pumice clasts are all sub-rounded	Yes	**No**	Yes	Yes	Yes	Yes
Very poorly segregated pumice clasts	Yes	**No**	**No**	Yes, if multiple pulses	**No**	**No**
Lithic clasts over entire stratigraphy	Yes, if multiple pulses	Yes, if multiple pulses	**No**	Yes, if multiple pulses	Yes	Yes
Presence of very fine particles in main deposit body	Yes, if multiple pulses	Yes, if aggregates	Yes, if multiple pulses	Yes, if multiple pulses	**No**	**No**
Resedimented bioclasts only at top of deposit	Yes	Yes	Yes	Yes	**No**	**No**

Note: Shaded columns for preferred interpretation.

runout, and when accelerating downslope (e.g., Piper et al., 1999) they commonly incorporate abundant bioclasts from soft hemipelagic substrates into the bulk of the flow (e.g., Trofimovs et al., 2006, 2008). The absence of bioclasts in subunit 1 is a major argument against subunit 1 being either a primary or nonprimary volcaniclastic turbidite. Therefore, turbidity currents may have been initiated at the island during this eruption, but they apparently did not reach Site U1396, possibly because of their lateral deflection into large canyons that run parallel to the ridge where Site U1396 is situated (Fig. 1).

Pyroclastic Fallout onto Water

Several observations can be used to assess whether the deposit was formed by pyroclastic fallout onto water (Table 1). The poor sorting (>12 phi of range in grain size) of this deposit, and the presence of multiple grain-size modes and subrounded pumice clasts are atypical of tephra-fall deposits (e.g., Walker and Croasdale, 1971). Furthermore, the thickness of the stratified pumice lapilli-ash is 1.2 m; this is quite thick considering its distance of >35 km from the presumed vent. Marine tephra beds derived from pyroclastic fall onto water associated with the Pinatubo eruption in 1991 (volcanic explosivity index [VEI] 6) and from the 1875 eruption that produced Askja Unit D (VEI 5) produced deposits that are only 20%–33% of the thickness of the stratified pumice lapilli-ash at an equal distance downwind from the vent (Paladio-Melosantos et al., 1996; Carey et al., 2010). The total thickness of the four Plinian-phase deposits of the 1815 Tambora eruption (VEI 7) would match the thickness of the stratified pumice lapilli-ash at the same distance from the vent (Self et al., 1984; Sigurdsson and Carey, 1989), but an eruption of such a scale on Montserrat would probably have produced substantial pyroclastic density currents and lahars, and those turbidity currents and/or hyperpycnal flows would have been likely to reach Site U1396 and form very thick deposits.

Pyroclastic fall at this distance from source would also normally deliver ash and small lapilli at ambient temperature (e.g., Carey et al., 1996); thus pumice lapilli would initially float and create rafts. Cold waterlogging of the studied pumice clasts requires 0–33 h (average is 5 h; this does not include outliers at 60–180 h), which is more than sufficient to sieve most of the dense lithic clasts and crystal fragments from the raft under wave motion (Carey et al., 2001; Jutzeler, 2015). Early release of dense clasts from the raft into water would produce a basal dense-clast-rich layer on the seafloor (Ledbetter and Sparks, 1979), which is not present in the stratified pumice lapilli-ash.

Implications of Subrounded Pumice Clasts

All pumice clasts from this study are subrounded, implying low to moderate abrasion during transport. Reworking in the surf zone is very efficient in rounding pumice (Manville et al., 2002, 2010). However, resedimentation of material from above-wave-base deposits implies efficient mixing with the substrate, which does not match the homogeneous composition of pumice clasts present in the stratified pumice lapilli-ash. The stratified pumice lapilli-ash could be the result of mass wasting of a submarine delta formed by a subaerial pyroclastic density current, although in that case, a large-volume, eruption-fed deposit would be expected to occur at Site U1396 as well. In contrast to transport in gas-supported pyroclastic density currents, subaqueous turbidity currents are supported by water, which is thought to be dense and viscous enough to buffer most clast-to-clast collisions (White, 2000). Therefore, an aqueous turbidity current is not expected to easily produce subrounded pumice clasts. Moreover, we consider a deep submarine eruption from Montserrat to be unlikely; if one happened, it would produce angular pumice clasts, make a deposit poor in fines, and probably involve some dispersal by turbidity currents (White, 2000; Kano, 2003; Allen and McPhie, 2009; Jutzeler et al., 2014b). Two main processes are known to efficiently round pumice clasts with minimal mixing with other deposits. (1) This first is pumice raft abrasion. Gentle wave-induced collisions mostly produce glass shards and liberate minor volumes of crystal fragments (Jutzeler et al., 2014a; Jutzeler, 2015). This mechanism would form a deposit of mostly glass fragments "milled" from pumice, but the U1396 deposits have abundant lithic clasts and crystal fragments throughout, which are not concentrated in a basal layer (Fig. 2). This unit is thus unlikely to have been derived from a raft (Table 1). (2) The second is a subaerial eruption-column collapse followed by particle transport in subaerial pyroclastic density currents. This process efficiently rounds pumice clasts (Manga et al., 2011; Kueppers et al., 2012) while also producing abundant crystal fragments and glass shards (Walker, 1972, 1983). From these considerations, initial transport by pyroclastic density currents is the best hypothesis to interpret subrounded pumice clasts in a very poorly sorted and stratified deposit that does not include a basal dense-clast-rich layer.

Pyroclastic Density Currents over Water

Explosive arc volcanism in coastal environments typically delivers a large fraction of pyroclasts directly to the ocean (Sigurdsson et al., 1980; Trofimovs et al., 2008; Wetzel, 2009; Manville et al., 2010). Pumice-rich pyroclastic density currents can have runout distances of tens of kilometers, sufficient to reach well beyond the shorelines of many islands. A majority of the recent collapsed domes at Montserrat were transferred into the sea (Trofimovs et al., 2008, 2012; Le Friant et al., 2009, 2010), demonstrating efficient transfer of pyroclasts to the submarine volcanic apron. Upon reaching the ocean, part of the pyroclastic density current may continue to travel across the water surface. The known maximum runout distances of pyroclastic density currents over water (20–80 km; Yokoyama, 1974; Fisher et al., 1993; Carey et al., 1996; Allen and Cas, 2001; Maeno and Taniguchi, 2007) show that Site U1396 is at a reasonable distance from Montserrat to collect products from large pumice-rich pyroclastic density currents (Table 1). This comparison also implies that this deposit is associated with an erupted volume similar to those that accompany caldera collapse. Upon reaching the ocean, pyroclastic density currents are subject to flow separation, in which at least a fraction of the high-clast concentration part (the bed load) enters the sea and transforms into a water-supported subaqueous turbidity current, or it drops its particles onto the shallow seafloor near the shore (Cas and Wright, 1991; Mandeville et al., 1996; Legros and Druitt, 2000; Freundt, 2003; Trofimovs et al., 2006, 2008, 2012; Jutzeler et al., 2014c). The dilute lower-density upper part of pyroclastic density currents is prone to remain subaerial (Fig. 16), running above the water interface until its energy is fully dissipated by areal dispersal, clast loss, turbulent mixing, lofting of secondary plumes, and cooling (Carey et al., 1996; Burgisser, 2005; Dufek and Bergantz, 2007; Dufek et al., 2009). Steam is thought to be continuously produced at the base of the pyroclastic density current by the inverse Leidenfrost effect (Hall et al., 1969), which minimizes the loss of kinetic energy by reducing basal flow friction, and minimizes heat loss by reducing interaction of the pyroclastic density current with seawater (Allen and Cas, 2001). In addition, steam explosions from contact between pyroclastic material and seawater may enhance the lateral momentum of the flow (Dufek et al., 2007). Apart from substantial loss of coarse lithic clasts (Allen and Cas, 2001; Burgisser, 2005; Dufek and Bergantz, 2007; Dufek et al., 2009) released into water, Allen and Cas (2001) did not report substantial componentry modification after flow over water, and Maeno and Taniguchi (2007) showed that small lithic clasts are present in subaerial deposits derived from transport >55 km over water. Hot (>100 °C) pumice clasts are likely to get quickly waterlogged (this study; Whitham and Sparks,

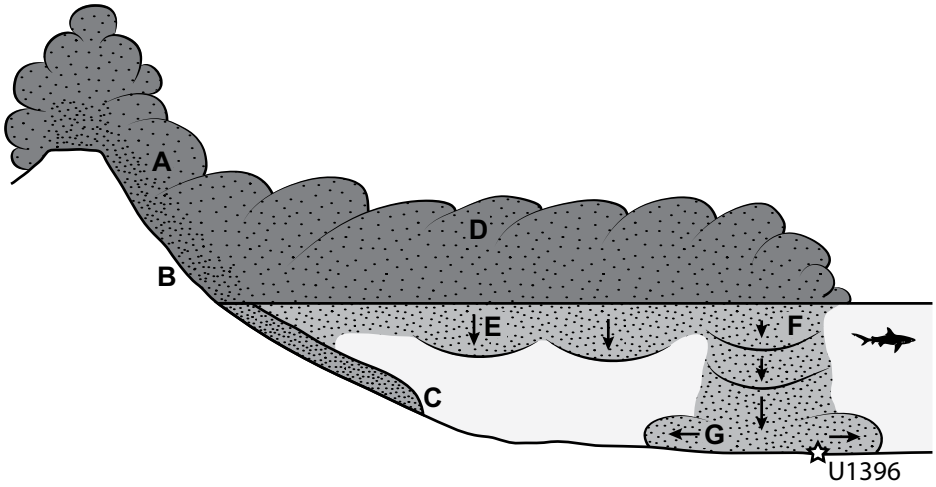

Figure 16. Cartoon summarizing the transport processes; not at scale. Pyroclastic density currents (dark gray) are generated at vent (A), flow downslope the volcano (B), possibly enter the sea at the shoreline and create turbidity currents (medium gray) that will not reach Site U1396 (C), travel over water, expand (D) and release clasts on the way (E), and finally undergo submarine settling of the pyroclasts and vertical plumes (density currents) of extremely fine particles (light gray; F). Lateral, seafloor-hugging turbidity currents (G) are created by deflection of groups of settling clasts arriving at the seafloor. Note that there is no information on the elevation of the vent.

1986; Dufek et al., 2007; Allen et al., 2008). Loss of clasts, production of steam at the base of the flow, steam explosions, and hot gas buoyancy will all contribute to flow inflation and lofting, and therefore dilution of the flow (Fig. 16). Production of steam and cooling of the pyroclastic density current will trigger ash aggregation (Carey et al., 1996), allowing part of the ash in atmospheric plumes to rapidly settle onto the sea surface together with the coarser clasts. Such moisture-aggregated particles will disaggregate when dropped onto water, releasing fine to extremely fine ash particles. The stratification of the pumice lapilli-ash implies multiple pulses of sedimentation, which commonly occur during pumice-forming explosive eruptions and during emplacement of pumice-rich pyroclastic density currents (Table 1).

Particle Waterlogging and Submersion

Considering initial transport by a pyroclastic density current over the sea, considerable sorting of particles is likely to occur at the water surface, where pumice clasts waterlog at a rate that depends on their temperature, permeability, porosity, and size (this study; Whitham and Sparks, 1986; White et al., 2001; Manville et al., 2002). The clasts with a longer floating time, such as coarse pumice clasts that need substantial time to waterlog even if partly waterlogged when hot (Whitham and Sparks, 1986), are likely to have been transported by surface ocean currents and deposited elsewhere. For instance, dispersion of pumice rafts by surface ocean currents and wind on the water surface is relatively quick, with an average worldwide rate at 0.1–0.3 m/s, corresponding to 9–26 km/d (Jutzeler et al., 2014a). Alternatively, coarse pumice clasts may have not been produced, or were deposited closer to vent. Similarly, the absence of very coarse lithic clasts can be explained by the long over-water distance, preventing any local entrainment of large clasts the depositional site. The largest and most dense clasts would have been deposited closer to shore, resulting in proportional enrichment in small pumice lapilli and fines in distal facies (e.g., Burgisser, 2005; Dufek and Bergantz, 2007; Maeno and Taniguchi, 2007; Dufek et al., 2009).

Settling of pyroclasts from pyroclastic density currents that travel over water is likely to create seafloor deposits that can be distinguished from those formed by other transport processes (Mandeville et al., 1994, 1996; Carey et al., 1996; Table 1). Here, we compare stratified pumice lapilli-ash facies with known products from subaerial pyroclastic density currents; subsequent modifications associated with transport in water are dealt in the next section. The stratified pumice lapilli-ash at Site U1396 is 1.2 m thick, suggesting input from currents that transported a substantial volume of clasts over the same location, which is typical of pyroclastic density currents. The modes of the grain-size distribution do not change through the unit (though mode amplitudes do), implying supply of similar material and therefore a common fragmentation history. The stratified pumice lapilli-ash contains lithic clasts and crystal fragments that are present through most of its thickness, and they did not preferentially accumulate at the base. That pattern indicates that, at least for the clasts present in the deposit, there was no substantial decoupling between pumice and lithic clasts during final sedimentation, and thus a very short period (seconds) when pumice clasts remained at the water surface. To match this coupling between dense clasts and pumice clasts in the resulting deposit, the pumice clasts must still have been hot when they landed on water, allowing them to very quickly become waterlogged and sink (Figs. 9 and 13). Only pyroclastic density currents can bring hot clasts tens of kilometers from a vent (e.g., Carey et al., 1996). The settling speed is ~0.1 m/s for an average-size (3 mm) water-saturated pumice clast, and it would have settled through 900 m of water in 2.5 h. Considering a generous 0.1 m/s as average bulk lateral velocity for ocean currents through the entire water column, the maximum lateral dispersal of pumice clasts is thus ~0.9 km, which is small compared to the ~35 km distance from the hypothesized source.

Vertical Settling of Particles

Offshore release of pyroclasts from pyroclastic density currents will affect large volumes of the ocean. Submerged pyroclasts will overall be carried downward under gravity (Fig. 16). For individually settling particles, efficient hydraulic sorting develops for all clasts as a function of their density, size, and shape (Clift et al., 1978; Cashman and Fiske, 1991; Manville et al., 2002; Dellino et al., 2005; Burgisser and Gardner, 2006; Barreyre et al., 2011; Jutzeler et al., 2015b). Sorting depends strongly on the type of transport, whether they settle as discrete particles (e.g., Cashman and Fiske, 1991) or are carried downward in plumes (Carey, 1997; Manville and Wilson, 2004; Jacobs et al., 2015). Initiation of vertical plumes is most efficient for high concentrations of extremely fine-ash particles (<63 μm), and velocities can be 1–3 orders of magnitude larger than the settling speed of single particles (Manville and Wilson, 2004; Jacobs et al., 2015). It is unclear whether very fine- to coarse-ash particles (63–710 μm) of the stratified pumice lapilli-ash experienced transport through vertical plumes or settled as individual particles. Our settling experiments did not show persistence of high-speed plumes over more than a few tens of centimeters for this grain size range, although the experimental load may not have reached critical clast concentration and/or volume required to fully represent this phenomenon. Moreover, prolonged input of

new particles at the water surface may also favor sustained vertical plumes.

The stratified pumice lapilli-ash consists of mixed components and has multiple grain-size modes, which makes assessing its sorting complicated (Table 1). There are consistent grain-size modes throughout the stratified pumice lapilli-ash, but large variations in modal grain-size amplitudes reflect efficient density grading over the entire range of grain sizes. The pumice clasts themselves are not graded by size or porosity, but small particles show density grading. This cryptic grading is not apparent to the naked eye, but was identified with the aid of detailed componentry and stereomicroscope grain-size analyses. The increase in abundance of the extremely fine-ash particles upward in the stratigraphy strongly suggests an overall progressive aggradation simultaneous with hydraulic sorting. The fine-grained intervals separating the three subunits suggest at least three pulses of sedimentation, and the stratified subunit 2 is likely to represent three pulses itself, making this deposit the product of five pulses of sedimentation. The minimum time between pulses of sedimentation can be broadly estimated by the settling speed of the particles present in the fine-grained beds. Using settling experiment data (our data; Cashman and Fiske, 1991) with a settling speed of 0.06–0.015 m/s for medium-sized ash particles, we estimate a total maximum settling time of 4–17 h. This time neglects enhanced settling by plumes, which we infer to have chiefly affected smaller particles.

The gradation from framework-supported to matrix-supported stratified pumice lapilli-ash may be related to the different settling speeds of particles. The lack of extremely fine ash particles in the bulk of subunit 1 reflects settling in a clear water environment, with coarse clasts strongly outrunning extremely small clasts that were deposited last (e.g., Ledbetter and Sparks, 1979). In contrast, pumice clasts and medium-ash particles of subunits 2 and 3 settled through, and incorporated billowing, slowly settling particulate plumes and/or slowly settling particles to produce an overall poorly sorted deposit (Fig. 16). The cryptic grading in medium- to extremely fine-ash particles through subunit 2 and 3 indicates that fine particles experienced hydraulic sorting during downward transport. This emplacement of subrounded pumice clasts and dense clasts in "dirty" water supports the rapid (<2 d; see earlier) arrival of new pulses of pyroclastic density currents over Site U1396, producing several pulses of settling in water. The presence of pumice clasts in all levels of subunits 2 and 3 suggests mixing of some fast-settling pumice clasts with slow-settling fine particles (Fisher, 1965). Delayed deposition of the fine particles also implies that they were not coupled with the coarse clasts during their settling through water. They may have been deposited onto water at nearby sites by the pyroclastic density currents and then laterally transported in the water column by ocean currents to their resting place. These interpretations are further supported by experimental and theoretical results showing that the modal grain size of pumice clasts and the modal grain size of crystal fragments are not at hydraulic equivalence (Fig. 12).

Deflection of Vertical Plumes

Lateral deflection of plumes (Fig. 16) is expected when they reach the seafloor and spread laterally as density currents (Manville and Wilson, 2004), and these currents would have intercepted particles from vertically descending plumes before they reached the seafloor. The perfect match in stratigraphy of the stratified pumice lapilli-ash across two drill holes situated 40 m apart is consistent with such a laterally deflected transport mechanism. The restriction of foraminifera tests to the uppermost part of the unit suggests entrainment of bioclasts from the water column into the billowing ash plumes during the final stage of deposition. Late deposition of these bioclasts within the stratified pumice lapilli-ash unit is also favored by the near-neutral buoyancy of the bioclasts.

Posteruption Reworking

The absence of an uppermost fine-grained top generated by slow-settling particles (commonly the finest ash), with instead an abrupt transition to overlying hemipelagic mud, may reflect ocean currents affecting the water column containing the ash plume so that the last-descending ash was transported away from Site U1396. Alternatively, local bottom currents may have eroded an initially deposited extremely fine ash top. Sparse isolated pumice clasts in the first few centimeters of the overlying hemipelagic mud (Fig. 3) suggest that small-scale mass wasting or erosion by bottom currents occurred upslope. The absence of burrows may be related to the coarseness of the unit, although deposition of such a thick volcaniclastic unit would certainly have affected benthic organisms (Wetzel, 2009), which may have taken a long time to recolonize this area after the eruption. However, at the Havre submarine volcano, benthic fauna recolonized very quickly (<3 yr) after a submarine eruption that deposited units of pumice clasts and glass shards (Soule and Carey, 2015).

Emergence of Montserrat

The date at which an island first grows above sea level is difficult to assess from the on-land rock record because the oldest rocks are commonly buried beneath younger eruption products. The oldest volcanic rock on Montserrat is 2.6 Ma (Harford et al., 2002), but it is unlikely to have formed at the time the island first appeared. In contrast, offshore drilling allows stratigraphic reconstruction of the main explosive events from an island. This study shows that the stratified pumice lapilli-ash formed at ca. 4 Ma was generated by powerful pyroclastic density currents that could travel for tens of kilometers over water. Such volcanic activity records large-magnitude, silicic volcanic eruptions that may include caldera-forming episodes. Eruption from a submerged vent is unlikely for several reasons. First, a deep-water (vent at >200 m below sea level) explosive eruption cannot produce a high enough eruption column to breach the water surface and generate powerful subaerial pyroclastic density currents that would travel laterally over water (Head and Wilson, 2003; Allen and McPhie, 2009). Second, a shallow-water (vent at <200 m below sea level) explosive eruption would be phreatoplinian in style (e.g., Wilson, 2001), and its corresponding products would be much finer grained than the studied deposit. Finally, the stratigraphy of U1396 shows several beds beneath and above the stratified pumice-lapilli-ash unit that contain similar white pumice clasts. These beds are normally graded and probably represent deposits from pyroclastic fall onto water, i.e., consistent with a subaerial vent. Therefore, the stratified pumice lapilli-ash is interpreted to record a subaerial eruption, bringing the emergence age of Montserrat to at least ca. 4 Ma.

Toward a General Understanding of the Behavior of Pumice in Water

The distinctive short flotation of the cold pumice clasts suggests that they probably have much higher permeability compared to most pumice clasts (e.g., Klug and Cashman, 1996). Interestingly, White et al. (2001) showed large variations in flotation time within populations of pumice clasts (Fig. 14) from the 232 A.D. Taupo Plinian eruption (Hogg et al., 2012), implying large variations in vesicularity (68–84 vol%; Houghton et al., 2010) and permeability. Despite the inferred high permeability, the pumice clasts of the stratified pumice lapilli-ash have a mean porosity of ~74%, similar to typical pumice (Klug and Cashman, 1996). High permeability suggests fully connected vesicles and few bubble wall constrictions (e.g., vesicles with bottleneck shape), which is supported by SEM and microtomography images (Fig. 7). Type 1 and type 2 pumices have similar vesicularity and chiefly differ in the amount of strain that leads to bubble elongation during ascent in the conduit

(e.g., Klug and Cashman, 1996). The presence of the same vesicle mode in all three types of pumice (at 2–4 μm; Fig. 8), despite large differences in amplitude of each mode, and pockets of type 3 pumice texture within type 2 pumice imply spatially variable bubble nucleation and/or elongation. Domains rich in very small vesicles may represent more viscous melt areas that hindered bubble growth, or regions with lower volatile contents that experienced delayed nucleation. Alternatively, they may be zones where melt quenched earlier, effectively stopping vesicle growth. Quenching occurs in response to fast cooling (in air or water) and may occur at the rims of clasts or adjacent to cracks in the pumice clasts, with the core of the pumice being initially thermally insulated from inward cooling (Kano et al., 1994; Manville et al., 1998). Quenching by water may occur at the vent (aquifer, crater lake, shallow-water eruption), or when a pyroclastic density current reaches the sea; both are possible for this deposit.

Cold experiments showed a strong relationship between flotation time and pumice porosity (Fig. 13), whereas previous studies on pumice clasts from Taupo and the Minoan eruptions (Whitham and Sparks, 1986; White et al., 2001) showed a strong relationship with the clast size (Fig. 14). Differences in the rate of waterlogging of cold pumice may vary strongly depending on the texture of the pumice (e.g., tube pumice, isolated pores, quenched margins, etc.). The quick waterlogging of most of our cold pumice clasts compared to measurements from other studies may suggest they are a highly permeable subpopulation of an original pumice clast population with a wider range in permeability, therefore making the small variations in size among these pumice clasts less relevant to settling behavior than their permeability values. The cold flotation experimental data on isolated pumice clasts distributed within hemipelagic mud in cores U1396-8H and 9H (0.7–0.8 Ma; Expedition 340 Scientists, 2012), and thought to have been settled from pumice rafts, also have a wide range in flotation times, from minutes to many days (Fig. 14).

In our hot experiments, the rate of waterlogging of hot pumice clasts was a function of their size (Fig. 13), as described for other pumice samples by Dufek et al. (2007) (Fig. 15). In contrast, Whitham and Sparks (1986) and Allen et al. (2008) found that hot pumice waterlogging was a function of the clast's porosity and permeability. This difference may be related to sampling bias in our pumice, which are probably all very permeable (see previous discussion). The relatively slow sinking of hot pumice clasts in this study (Fig. 15) compared to those from Medicine Lake studied by Dufek et al. (2007) is surprising, especially considering our pumice clasts sank very quickly during the cold experiments. We followed the same procedures as Dufek et al. (2007) except for heating our pumice to 600 °C instead of 500 °C. For high temperatures (>100–700 °C), Whitham and Sparks (1986) found a linear relationship between the degree of waterlogging and the initial temperature of the pumice clast, and so our experiments should have shown a faster rate of waterlogging instead. This discrepancy between different samples points toward the role of porosity and/or permeability in the rate of pumice waterlogging (Whitham and Sparks, 1986; Allen et al., 2008).

CONCLUSIONS

Expedition IODP 340 cored a 1.2-m-thick stratified pumice lapilli-ash dated at ca. 4 Ma in two holes at 123 m below seafloor at Site U1396 southwest offshore Montserrat Island (Lesser Antilles). The unit consists of a complex facies that records marine deposition of pyroclasts transported ~35 km southwestward from Montserrat. This pumice-rich unit has the geochemical signature of Soufrière Hills (Montserrat) and was probably emplaced during a voluminous, subaerial caldera-forming eruption.

Based on sedimentological characteristics, we infer that the very poor sorting of this deposit resulted from mixing of various particles delivered during pulses of sedimentation, rather than from an inability of the transport and sedimentation processes *per se* to sort the particles. We interpret this facies to have formed by a two-step sedimentation process involving pumice-rich pyroclastic density currents traveling over water, followed by vertical transport of particles through the water column by discrete settling and vertical plumes that were laterally deflected when they reached the seafloor. This is the first study characterizing such a deposit.

At Site U1396, the subrounded pumice clasts were hot enough to quickly waterlog, and they remained coupled with the coarse lithic clasts and crystal fragments during submersion in water. Fast-sinking coarse pumice and lithic clasts form the base of the framework-supported subunit 1, which is topped with medium- and extremely fine-ash particles. The two overlying subunits are matrix-supported units, with inferred density sorting yielding an upward increase in abundance of pumice clasts and extremely fine glass shards at the expense of dense lithic clasts and crystal fragments. Gradational stratification and poor sorting together with density grading strongly suggest that mixtures of components settling at different velocities were introduced into the water column through several pulses associated with pyroclastic density currents traveling over water, to create an overall well-mixed, very poorly sorted deposit. The presence of fine particles that were overtaken, while they settled toward the seafloor, by successive arrivals of new coarse particles provides a sedimentation time frame suggesting the entire unit was formed in <2 d. Differential settling speeds that depend chiefly on grain size suggest that the coarse- and fine-ash particles may not have all been released onto the water surface at the same location by the pyroclastic density currents. Due to their slow settling speed, fine-ash particles have a longer residence time in the water column than do coarser pumice and lithic clasts. Thus, the fine ash was transported laterally a larger distance in the water column by ocean currents, and was probably initially deposited onto water further from the depositional site.

Flotation experiments from this study reveal that the pumice clasts from this deposit waterlog as a function of porosity and not according to their size when cold (20 °C), whereas hot pumice clasts (600 °C) sink as a function of their size. Discrepancies in the speed of waterlogging for these cold and hot pumice clasts compared with rates reported elsewhere highlight the need for further work on the processes of waterlogging. This study reveals effects of a complex interaction between coastal eruptions and the ocean, and the lack of previously reported deposits of this sort is inferred to reflect the paucity of marine volcaniclastic sediment cores thus far recovered. There is a need to better understand marine sedimentation processes in the context of coastal and island volcanism, which poses significant hazards to human populations.

ACKNOWLEDGMENTS

This work is based on piston cores collected during Integrated Ocean Drilling Program (IODP) 340. We thank the captain, crew, and technical staff of the R/V *JOIDES Resolution* for their high level of experience, which ensured recovery of high-quality cores. Jutzeler was funded by the Swiss National Science Foundation through grants PBSKP2_138556 and PBSKP2_145907, NERC Grant NEW314019, and a research grant from the University of Otago. ANZIC (Australia-New Zealand IODP Consortium) provided funding for Jutzeler to participate in the IODP 340 Expedition, and ECORD (European Consortium for Ocean Research Drilling) provided funding for travel to a postexpedition meeting. S. Allen and J. Trofimovs are thanked for their constructive reviews. We greatly acknowledge D. Parkinson (Advanced Light Source Berkeley), C. Thompson and A. Michalik (University of Southampton), S. Kearns (University of Bristol), A. Patel (University of California–Berkeley), S. MacLachlan (National Oceanography Centre, Southampton), and L. Easterbrook (University of Otago) for assistance in the laboratories.

REFERENCES CITED

Allen, S.R., and Cas, R.A.F., 2001, Transport of pyroclastic flows across the sea during the explosive rhyolitic eruption of the Kos Plateau Tuff, Greece: Bulletin of Volcanology, v. 62, p. 441–456, doi:10.1007/s004450000107.

Allen, S.R., and Freundt, A., 2006, Resedimentation of cold pumiceous ignimbrite into water: Facies transformations simulated in flume experiments: Sedimentology, v. 53, p. 717–734, doi:10.1111/j.1365-3091.2006.00790.x.

Allen, S.R., and McPhie, J., 2009, Products of Neptunian eruptions: Geology, v. 37, p. 639–642, doi:10.1130/G30007A.1.

Allen, S.R., and Stewart, A.L., 2003, Products of explosive subaqueous felsic eruptions based on examples from the Hellenic island arc, Greece, *in* White, J.D.L., Smellie, J.L., and Clague, D.A., eds., Explosive Subaqueous Volcanism: Washington, D.C., American Geophysical Union, p. 285–298, doi:10.1029/140GM19.

Allen, S.R., Fiske, R.S., and Cashman, K.V., 2008, Quenching of steam-charged pumice; implications for submarine pyroclastic volcanism: Earth and Planetary Science Letters, v. 274, p. 40–49, doi:10.1016/j.epsl.2008.06.050.

Allen, S.R., Fiske, R.S., and Tamura, Y., 2010, Effects of water depth on pumice formation in submarine domes at Sumisu, Izu-Bonin arc, western Pacific: Geology, v. 38, p. 391–394, doi:10.1130/G30500.1.

Allen, S.R., Freundt, A., and Kurokawa, K., 2012, Characteristics of submarine pumice-rich density current deposits sourced from turbulent mixing of subaerial pyroclastic flows at the shoreline: Field and experimental assessment: Bulletin of Volcanology, v. 74, p. 657–675, doi:10.1007/s00445-011-0553-1.

Barreyre, T., Soule, S.A., and Sohn, R.A., 2011, Dispersal of volcaniclasts during deep-sea eruptions: Settling velocities and entrainment in buoyant seawater plumes: Journal of Volcanology and Geothermal Research, v. 205, p. 84–93, doi:10.1016/j.jvolgeores.2011.05.006.

Boudon, G., Le Friant, A., Komorowski, J.-C., Deplus, C., and Semet, M.P., 2007, Volcano flank instability in the Lesser Antilles Arc: Diversity of scale, processes, and temporal recurrence: Journal of Geophysical Research, v. 112, p. B08205, doi:10.1029/2006JB004674.

Bouysse, P., and Westercamp, D., 1990, Subduction of Atlantic aseismic ridges and late Cenozoic evolution of the Lesser Antilles island arc: Tectonophysics, v. 175, p. 349–380, doi:10.1016/0040-1951(90)90180-G.

Briden, J.C., Rex, D.C., Faller, A.M., and Tomblin, J.F., 1979, K-Ar geochronology and palaeomagnetism of volcanic rocks in the Lesser Antilles island arc: Philosophical Transactions of the Royal Society of London, ser. A, Mathematical and Physical Sciences, v. 291, p. 485–528, doi:10.1098/rsta.1979.0040.

Bryan, S.E., Cook, A.G., Evans, J.P., Hebden, K., Hurrey, L., Colls, P., Jell, J.S., Weatherley, D., and Firn, J., 2012, Rapid, long-distance dispersal by pumice rafting: PLoS One, v. 7, p. e40583, doi:10.1371/journal.pone.0040583.

Burgisser, A., 2005, Physical volcanology of the 2,050 BP caldera-forming eruption of Okmok volcano, Alaska: Bulletin of Volcanology, v. 67, p. 497–525, doi:10.1007/s00445-004-0391-5.

Burgisser, A., and Gardner, J.E., 2006, Using hydraulic equivalences to discriminate transport processes of volcanic flows: Geology, v. 34, p. 157–160, doi:10.1130/G21942.1.

Campbell, S.D.G., Howells, M.F., Reedman, A.J., Whitham, A.G., and Sparks, R.S.J., 1987, Comment and reply on "Pumice": Bulletin of Volcanology, v. 49, p. 567–569, doi:10.1007/BF01080450.

Cantelli, A., Johnson, S., White, J.D.L., and Parker, G., 2008, Sediment sorting in the deposits of turbidity currents created by experimental modeling of explosive subaqueous eruptions: The Journal of Geology, v. 116, p. 76–93, doi:10.1086/524676.

Carey, R.J., Houghton, B.F., and Thordarson, T., 2010, Tephra dispersal and eruption dynamics of wet and dry phases of the 1875 eruption of Askja Volcano, Iceland: Bulletin of Volcanology, v. 72, p. 259–278, doi:10.1007/s00445-009-0317-3.

Carey, R.J., Wysoczanski, R., Wunderman, R., and Jutzeler, M., 2014, Discovery of the largest historic silicic submarine eruption: Eos, Transactions, American Geophysical Union, v. 95, p. 157–159, doi:10.1002/2014EO190001.

Carey, S., 1997, Influence of convective sedimentation on the formation of widespread tephra fall layers in the deep sea: Geology, v. 25, p. 839–842, doi:10.1130/0091-7613(1997)025<0839:IOCSOT>2.3.CO;2.

Carey, S., Sigurdsson, H., Mandeville, C., and Bronto, S., 1996, Pyroclastic flows and surges over water: An example from the 1883 Krakatau eruption: Bulletin of Volcanology, v. 57, p. 493–511, doi:10.1007/BF00304435.

Carey, S., Morelli, D., Sigurdsson, H., and Bronto, S., 2001, Tsunami deposits from major explosive eruptions: An example from the 1883 eruption of Krakatau: Geology, v. 29, p. 347–350, doi:10.1130/0091-7613(2001)029<0347:TDFMEE>2.0.CO;2.

Carey, S.N., 2000, Volcaniclastic sedimentation around island arcs, *in* Sigurdsson, H., Houghton, B.F., McNutt, S.R., Rymer, H., and Stix, J., eds., Encyclopedia of Volcanoes: San Diego, California, Academic Press, p. 627–642.

Carey, S.N., and Sigurdsson, H., 1980, The Roseau ash: Deep-sea tephra deposits from a major eruption on Dominica, Lesser Antilles arc: Journal of Volcanology and Geothermal Research, v. 7, p. 67–86, doi:10.1016/0377-0273(80)90020-7.

Cas, R.A.F., and Wright, J.V., 1991, Subaqueous pyroclastic flows and ignimbrites: An assessment: Bulletin of Volcanology, v. 53, p. 357–380, doi:10.1007/BF00280227.

Cashman, K.V., and Fiske, R.S., 1991, Fallout of pyroclastic debris from submarine volcanic eruptions: Science, v. 253, p. 275–280, doi:10.1126/science.253.5017.275.

Cassidy, M., Taylor, R.N., Palmer, M.R., Cooper, R.J., Stenlake, C., and Trofimovs, J., 2012, Tracking the magmatic evolution of island arc volcanism: Insights from a high-precision Pb isotope record of Montserrat, Lesser Antilles: Geochemistry Geophysics Geosystems, v. 13, doi:10.1029/2012GC004064.

Cassidy, M., Trofimovs, J., Palmer, M.R., Talling, P.J., Watt, S.F.L., Moreton, S.G., and Taylor, R.N., 2013, Timing and emplacement dynamics of newly recognised mass flow deposits at ~8–12ka offshore Soufrière Hills volcano, Montserrat: How submarine stratigraphy can complement subaerial eruption histories: Journal of Volcanology and Geothermal Research, v. 253, p. 1–14, doi:10.1016/j.jvolgeores.2012.12.002.

Cassidy, M., Trofimovs, J., Watt, S.F.L., Palmer, M.R., Taylor, R.N., Gernon, T.M., Talling, P.J., and Le Friant, A., 2014a, Multi-stage collapse events in the South Soufriere Hills, Montserrat, as recorded in marine sediment cores, *in* Wadge, G., Robertson, R.E.A., and Voight, B., eds., The Eruption of Soufriere Hills Volcano, Montserrat, 2000 to 2010: Geological Society of London Memoir 39, p. 383–397, doi:10.1144/M39.20.

Cassidy, M., Watt, S.F.L., Palmer, M.R., Trofimovs, J., Symons, W., Maclachlan, S.E., and Stinton, A.J., 2014b, Construction of volcanic records from marine sediment cores; a review and case study (Montserrat, West Indies): Earth-Science Reviews, v. 138, p. 137–155, doi:10.1016/j.earscirev.2014.08.008.

Cassidy, M., Watt, S.F.L., Talling, P.J., Palmer, M.R., Edmonds, M., Jutzeler, M., Wall-Palmer, D., Manga, M., Coussens, M., Gernon, T., Taylor, R.N., Michalik, A., Inglis, E., Breitkreuz, C., Le Friant, A., Ishizuka, O., Boudon, G., McCanta, M.C., Adachi, T., Hornbach, M.J., Colas, S.L., Endo, D., Fujinawa, A., Kataoka, K.S., Maeno, F., Tamura, Y., and Wang, F., 2015, Rapid onset of mafic magmatism facilitated by volcanic edifice collapse: Geophysical Research Letters, v. 42, p. 4778–4785, doi:10.1002/2015GL064519.

Clift, R., Grace, J.R., and Weber, M.E., 1978, Bubbles, Drops, and Particles: Mineola, New York, Dover Publications, 381 p.

Cole, R.B., and DeCelles, P.G., 1991, Subaerial to submarine transitions in early Miocene pyroclastic flow deposits, southern San Joaquin basin, California: Geological Society of America Bulletin, v. 103, p. 221–235, doi:10.1130/0016-7606(1991)103<0221:STSTIE>2.3.CO;2.

Cole, P.D., Calder, E.S., Druitt, T.H., Hoblitt, R., Robertson, R., Sparks, R.S.J., and Young, S.R., 1998, Pyroclastic flows generated by gravitational instability of the 1996–97 lava dome of Soufrière Hills Volcano, Montserrat: Geophysical Research Letters, v. 25, p. 3425–3428, doi:10.1029/98GL01510.

Coussens, M., Wall-Palmer, D., Talling, P.J., Watt, S.F.L., Cassidy, M., Jutzeler, M., Clare, M.A., Hunt, J.E., Manga, M., Gernon, T.M., Palmer, M.R., Hatter, S.J., Boudon, G., Endo, D., Fujinawa, A., Hatfield, R., Hornbach, M.J., Ishizuka, O., Kataoka, K., Le Friant, A., Maeno, F., McCanta, M., and Stinton, A.J., 2016, The relationship between eruptive activity, flank collapse, and sea level at volcanic islands: A long-term (>1 Ma) record offshore Montserrat, Lesser Antilles: Geochemistry Geophysics Geosystems, v. 17, no. 7, doi:10.1002/2015GC006053.

Dellino, P., Mele, D., Bonasia, R., Braia, G., La Volpe, L., and Sulpizio, R., 2005, The analysis of the influence of pumice shape on its terminal velocity: Geophysical Research Letters, v. 32, p. L21306, doi:10.1029/2005GL023954.

Deplus, C., Le Friant, A., Boudon, G., Komorowski, J.C., Villemant, B., Harford, C., Ségoufin, J., and Cheminée, J.L., 2001, Submarine evidence for large-scale debris avalanches in the Lesser Antilles Arc: Earth and Planetary Science Letters, v. 192, p. 145–157, doi:10.1016/S0012-821X(01)00444-7.

Dufek, J., and Bergantz, G.W., 2007, Dynamics and deposits generated by the Kos Plateau Tuff eruption: Controls of basal particle loss on pyroclastic flow transport: Geochemistry Geophysics Geosystems, v. 8, p. Q12007, doi:10.1029/2007GC001741.

Dufek, J., Manga, M., and Staedter, M., 2007, Littoral blasts: Pumice-water heat transfer and the conditions for steam explosions when pyroclastic flows enter the ocean: Journal of Geophysical Research–Solid Earth and Planets, v. 112, p. B11201, doi:10.1029/2006JB004910.

Dufek, J., Wexler, J., and Manga, M., 2009, Transport capacity of pyroclastic density currents: Experiments and models of substrate-flow interaction: Journal of Geophysical Research–Solid Earth and Planets, v. 114, p. B11203, doi:10.1029/2008JB006216.

Expedition 340 Scientists, 2012, Lesser Antilles Volcanism and Landslides: Implications for Hazard Assessment and Long-Term Magmatic Evolution of the Arc: Integrated Ocean Drilling Program Preliminary Report 340, 86 p., doi:10.2204/iodp.pr.340.2012.

Expedition 350 Scientists, 2014, Izu-Bonin-Mariana Rear Arc: The Missing Half of the Subduction Factory: Integrated Ocean Drilling Program Preliminary Report 350, 64 p., doi:10.14379/iodp.pr.350.2014.

Fisher, R.V., 1965, Settling velocity of glass shards: Deep-Sea Research and Oceanographic Abstracts, v. 12, p. 345–353, doi:10.1016/0011-7471(65)90006-9.

Fisher, R.V., Orsi, G., Ort, M., and Heiken, G., 1993, Mobility of a large-volume pyroclastic flow—Emplacement of the Campanian ignimbrite, Italy: Journal of Volcanology and Geothermal Research, v. 56, p. 205–220, doi:10.1016/0377-0273(93)90017-L.

Fiske, R.S., Cashman, K.V., Shibata, A., and Watanabe, K., 1998, Tephra dispersal from Myojinsho, Japan, during its shallow submarine eruption of 1952–1953: Bulletin of Volcanology, v. 59, p. 262–275, doi:10.1007/s004450050190.

Fiske, R.S., Naka, J., Iizasa, K., Yuasa, M., and Klaus, A., 2001, Submarine silicic caldera at the front of the Izu-Bonin arc, Japan; voluminous seafloor eruptions of rhyolite pumice: Geological Society of America Bulletin, v. 113, p. 813–824, doi:10.1130/0016-7606(2001)113<0813:SSCATF>2.0.CO;2.

Freundt, A., 2003, Entrance of hot pyroclastic flows into the sea: Experimental observations: Bulletin of Volcanology, v. 65, p. 144–164.

Hall, R.S., Board, S.J., Clare, A.J., Duffey, R.B., Playle, T.S., and Poole, D.H., 1969, Inverse Leidenfrost phenomenon: Nature, v. 224, p. 266–267, doi:10.1038/224266a0.

Harford, C.L., Pringle, M.S., Sparks, R.S.J., and Young, S.R., 2002, The volcanic evolution of Montserrat using $^{40}Ar/^{39}Ar$ geochronology, *in* Druitt, T.H., and Kokelaar, B.P., eds., The Eruption of Soufriere Hills Volcano, Montserrat from 1995 to 1999: Bath, UK, Geologi-

cal Society Publishing House, p. 93–113, doi:10.1144/GSL.MEM.2002.021.01.05.

Hart, K., Carey, S., Sigurdsson, H., Sparks, R.S.J., and Robertson, R.E.A., 2004, Discharge of pyroclastic flows into the sea during the 1996–1998 eruptions of the Soufrière Hills volcano, Montserrat: Bulletin of Volcanology, v. 66, p. 599–614, doi:10.1007/s00445-004-0342-1.

Head, J.W., and Wilson, L., 2003, Deep submarine pyroclastic eruptions: Theory and predicted landforms and deposits: Journal of Volcanology and Geothermal Research, v. 121, p. 155–193, doi:10.1016/S0377-0273(02)00425-0.

Hogg, A., Lowe, D.J., Palmer, J., Boswijk, G., and Bronk Ramsey, C., 2012, Revised calendar date for the Taupo eruption derived by ^{14}C wiggle-matching using a New Zealand kauri ^{14}C calibration data set: The Holocene, v. 22, p. 439–449, doi:10.1177/0959683611425551.

Houghton, B.F., and Wilson, C.J.N., 1989, A vesicularity index for pyroclastic deposits: Bulletin of Volcanology, v. 51, p. 451–462, doi:10.1007/BF01078811.

Houghton, B.F., Carey, R.J., Cashman, K.V., Wilson, C.J.N., Hobden, B.J., and Hammer, J.E., 2010, Diverse patterns of ascent, degassing, and eruption of rhyolite magma during the 1.8ka Taupo eruption, New Zealand: Evidence from clast vesicularity: Journal of Volcanology and Geothermal Research, v. 195, p. 31–47, doi:10.1016/j.jvolgeores.2010.06.002.

Huppertz, T.J., and Piper, D.J.W., 2010, Interbedded late Quaternary turbidites and contourites in Flemish Pass, off southeast Canada: Their recognition, origin and temporal variation: Sedimentary Geology, v. 228, p. 46–60, doi:10.1016/j.sedgeo.2010.04.004.

Ito, M., 2002, Kuroshio current-influenced sandy contourites from the Plio-Pleistocene Kazusa forearc basin, Boso Peninsula, Japan, *in* Stow, D.A.V., Pudsey, C.J., Howe, J.A., Faugeres, J.-C., and Viana, A.R., eds., Deep-Water Contourite Systems; Modern Drifts and Ancient Series, Seismic and Sedimentary Characteristics: Bath, UK, Geological Society Publishing House, p. 421–432, doi:10.1144/GSL.MEM.2002.022.01.29.

Jacobs, C.T., Goldin, T.J., Collins, G.S., Piggott, M.D., Kramer, S.C., Melosh, H.J., Wilson, C.R.G., and Allison, P.A., 2015, An improved quantitative measure of the tendency for volcanic ash plumes to form in water; implications for the deposition of marine ash beds: Journal of Volcanology and Geothermal Research, v. 290, p. 114–124, doi:10.1016/j.jvolgeores.2014.10.015.

Jutzeler, M., 2015, Abrasion in pumice rafts, *in* International Union of Geodesy and Geophysics Conference, Abstract IUGG-1733, 26th IUGG general assembly 2015, Prague, Czech Republic, Prague Congress Centre, 22 June–2 July 2015; Earth and environmental sciences for future generations, 2015: Prague, Czech Republic, Conference: 26th International Union of Geodesy and Geophysics general assembly.

Jutzeler, M., Proussevitch, A.A., and Allen, S.R., 2012, Grain-size distribution of volcaniclastic rocks: 1. A new technique based on functional stereology: Journal of Volcanology and Geothermal Research, v. 239–240, p. 1–11, doi:10.1016/j.jvolgeores.2012.05.013.

Jutzeler, M., Marsh, R., Carey, R.J., White, J.D.L., Talling, P.J., and Karlstrom, L., 2014a, On the fate of pumice rafts formed during the 2012 Havre submarine eruption: Nature Communications, v. 5, p. 3660, doi:10.1038/ncomms4660.

Jutzeler, M., McPhie, J., and Allen, S., 2014b, Submarine eruption-fed and resedimented pumice-rich facies: The Dogashima Formation (Izu Peninsula, Japan): Bulletin of Volcanology, v. 76, p. 867, doi:10.1007/s00445-014-0867-x.

Jutzeler, M., McPhie, J., and Allen, S.R., 2014c, Facies architecture of a continental, below-wave-base volcaniclastic basin: The Ohanapecosh Formation, ancestral Cascades arc (Washington, USA): Geological Society of America Bulletin, v. 126, p. 352–376, doi:10.1130/B30763.1.

Jutzeler, M., White, J.D.L., Talling, P.J., McCanta, M., Morgan, S., Le Friant, A., and Ishizuka, O., 2014d, Coring disturbances in IODP piston cores with implications for offshore record of volcanic events and the Missoula megafloods: Geochemistry Geophysics Geosystems, v. 15, p. 3572–3590, doi:10.1002/2014GC005447.

Jutzeler, M., McPhie, J., and Allen, S.R., 2015a, Explosive destruction of a Pliocene hot lava dome underwater: Dogashima (Japan): Journal of Volcanology and Geothermal Research, v. 304, p. 75–81, doi:10.1016/j.jvolgeores.2015.08.009.

Jutzeler, M., McPhie, J., Allen, S.R., and Proussevitch, A.A., 2015b, Grain-size distribution of volcaniclastic rocks: 2. Characterizing grain size and hydraulic sorting: Journal of Volcanology and Geothermal Research, v. 301, p. 191–203, doi:10.1016/j.jvolgeores.2015.05.019.

Jutzeler, M., Talling, P.J., White, J.D.L., and Expedition 340 Scientists, 2016, Data report: Coring disturbances in IODP 340, a detailed list of intervals with fall-in and flow-in, *in* Le Friant, A., Ishizuka, O., Stroncik, N.A., and the Expedition 340 Scientists, eds., Proceedings Integrated Ocean Drilling Program Volume 340: Tokyo, Japan, Integrated Ocean Drilling Program Management International, Inc., p. 1–14.

Kano, K., 2003, Subaqueous pumice eruptions and their products; a review, *in* White, J.D.L., Smellie, J.L., and Clague, D.A., eds., Explosive Subaqueous Volcanism: Washington, D.C., American Geophysical Union, p. 213–229, doi:10.1029/140GM14.

Kano, K., Orton, G.J., and Kano, T., 1994, A hot Miocene subaqueous scoria-flow deposit in the Shimane Peninsula, SW Japan: Journal of Volcanology and Geothermal Research, v. 60, p. 1–14, doi:10.1016/0377-0273(94)90094-9.

Kataoka, K., 2005, Distal fluvio-lacustrine volcaniclastic resedimentation in response to an explosive silicic eruption: The Pliocene Mushono tephra bed, central Japan: Geological Society of America Bulletin, v. 117, p. 3–17, doi:10.1130/B25379.1.

Kataoka, K., and Nakajo, T., 2002, Volcaniclastic resedimentation in distal fluvial basins induced by large-volume explosive volcanism: The Ebisutoge-Fukuda tephra, Plio-Pleistocene boundary, central Japan: Sedimentology, v. 49, p. 319–334, doi:10.1046/j.1365-3091.2002.00445.x.

Kato, Y., 1987, Woody pumice generated with submarine eruption: Chishitsugaku Zasshi: Journal of the Geological Society of Japan, v. 93, p. 11–20, doi:10.5575/geosoc.93.11.

Klug, C., and Cashman, K.V., 1996, Permeability development in vesiculating magmas: Implications for fragmentation: Bulletin of Volcanology, v. 58, p. 87–100, doi:10.1007/s004450050128.

Klug, C., Cashman, K., and Bacon, C., 2002, Structure and physical characteristics of pumice from the climactic eruption of Mount Mazama (Crater Lake), Oregon: Bulletin of Volcanology, v. 64, p. 486–501, doi:10.1007/s00445-002-0230-5.

Kueppers, U., Putz, C., Spieler, O., and Dingwell, D.B., 2012, Abrasion in pyroclastic density currents: Insights from tumbling experiments: Physics and Chemistry of the Earth, Parts A/B/C, v. 45–46, p. 33–39, doi:10.1016/j.pce.2011.09.002.

Kutterolf, S., Schindlbeck, J.C., Scudder, R.P., Murray, R.W., Pickering, K.T., Freundt, A., Labanieh, S., Heydolph, K., Saito, S., Naruse, H., Underwood, M.B., and Wu, H., 2014, Large volume submarine ignimbrites in the Shikoku Basin; an example for explosive volcanism in the western Pacific during the late Miocene: Geochemistry Geophysics Geosystems, v. 15, p. 1837–1851, doi:10.1002/2014GC005263.

Lacroix, A., 1904, La Montagne Pelée et ses Éruptions: Paris, Masson et Cie, 662 p.

Larsen, G., Eiriksson, J., and Gudmundsdottir, E.R., 2014, Last millennium dispersal of air-fall tephra and ocean-rafted pumice towards the north Icelandic shelf and the Nordic seas, *in* Austin, W.E.N., Abbott, P.M., Davies, S.M., Pearce, N.J.G., and Wastegård, S., eds., Marine Tephrochronology: Geological Society of London Special Publication 398, p. 113–140, doi:10.1144/SP398.4.

Lebas, E., Le Friant, A., Boudon, G., Watt, S.F.L., Talling, P.J., Feuillet, N., Deplus, C., Berndt, C., and Vardy, M.E., 2011, Multiple widespread landslides during the long-term evolution of a volcanic island: Insights from high-resolution seismic data, Montserrat, Lesser Antilles: Geochemistry Geophysics Geosystems, v. 12, p. Q05006, doi:10.1029/2010GC003451.

Ledbetter, M.T., and Sparks, R.S.J., 1979, Duration of large-magnitude explosive eruptions deduced from graded bedding in deep-sea ash layers: Geology, v. 7, p. 240–244, doi:10.1130/0091-7613(1979)7<240:DOLEED>2.0.CO;2.

Le Friant, A., Harford, C.L., Deplus, C., Boudon, G., Sparks, R.S.J., Herd, R.A., and Komorowski, J.C., 2004, Geomorphological evolution of Montserrat (West Indies): Importance of flank collapse and erosional processes: Journal of the Geological Society of London, v. 161, p. 147–160, doi:10.1144/0016-764903-017.

Le Friant, A., Lock, E.J., Hart, M.B., Boudon, G., Sparks, R.S.J., Leng, M.J., Smart, C.W., Komorowski, J.C., Deplus, C., and Fisher, J.K., 2008, Late Pleistocene tephrochronology of marine sediments adjacent to Montserrat, Lesser Antilles volcanic arc: Journal of the Geological Society of London, v. 165, p. 279–289, doi:10.1144/0016-76492007-019.

Le Friant, A., Deplus, C., Boudon, G., Sparks, R.S.J., Trofimovs, J., and Talling, P., 2009, Submarine deposition of volcaniclastic material from the 1995–2005 eruptions of Soufriere Hills volcano, Montserrat: Journal of the Geological Society of London, v. 166, p. 171–182, doi:10.1144/0016-76492008-047.

Le Friant, A., Deplus, C., Boudon, G., Feuillet, N., Trofimovs, J., Komorowski, J.C., Sparks, R.S.J., Talling, P.J., Loughlin, S., Palmer, M., and Ryan, G., 2010, Eruption of Soufrière Hills (1995–2009) from an offshore perspective: Insights from repeated swath bathymetry surveys: Geophysical Research Letters, v. 37, p. L11307, doi:10.1029/2010GL043580.

Le Friant, A., Ishizuka, O., Boudon, G., Palmer, M.R., Talling, P.J., Villemant, B., Adachi, T., Aljahdali, M., Breitkreuz, C., Brunet, M., Caron, B., Coussens, M., Deplus, C., Endo, D., Feuillet, N., Fraas, A.J., Fujinawa, A., Hart, M.B., Hatfield, R.G., Hornbach, M., Jutzeler, M., Kataoka, K.S., Komorowski, J.C., Lebas, E., Lafuerza, S., Maeno, F., Manga, M., Martínez-Colón, M., McCanta, M., Morgan, S., Saito, T., Slagle, A., Sparks, S., Stinton, A., Stroncik, N., Subramanyam, K.S.V., Tamura, Y., Trofimovs, J., Voight, B., Wall-Palmer, D., Wang, F., and Watt, S.F.L., 2015, Submarine record of volcanic island construction and collapse in the Lesser Antilles arc: First scientific drilling of submarine volcanic island landslides by IODP Expedition 340: Geochemistry Geophysics Geosystems, v. 16, p. 420–442, doi:10.1002/2014GC005652.

Legros, F., and Druitt, T.H., 2000, On the emplacement of ignimbrite in shallow-marine environments: Journal of Volcanology and Geothermal Research, v. 95, p. 9–22, doi:10.1016/S0377-0273(99)00116-X.

Lowe, D.J., 2011, Tephrochronology and its application: A review: Quaternary Geochronology, v. 6, p. 107–153, doi:10.1016/j.quageo.2010.08.003.

Macdonald, R., Hawkesworth, C.J., and Heath, E., 2000, The Lesser Antilles volcanic chain: A study in arc magmatism: Earth-Science Reviews, v. 49, p. 1–76, doi:10.1016/S0012-8252(99)00069-0.

Maeno, F., and Taniguchi, H., 2007, Spatiotemporal evolution of a marine caldera-forming eruption, generating a low-aspect ratio pyroclastic flow, 7.3 ka, Kikai caldera, Japan: Implication from near-vent eruptive deposits: Journal of Volcanology and Geothermal Research, v. 167, p. 212–238, doi:10.1016/j.jvolgeores.2007.05.003.

Mandeville, C.W., Carey, S., Sigurdsson, H., and King, J., 1994, Paleomagnetic evidence for high-temperature emplacement of the 1883 subaqueous pyroclastic flows from Krakatau volcano, Indonesia: Journal of Geophysical Research, v. 99, p. 9487–9504, doi:10.1029/94JB00239.

Mandeville, C.W., Carey, S., and Sigurdsson, H., 1996, Sedimentology of the Krakatau 1883 submarine pyroclastic deposits: Bulletin of Volcanology, v. 57, p. 512–529, doi:10.1007/BF00304436.

Manga, M., Patel, A., and Dufek, J., 2011, Rounding of pumice clasts during transport: Field measurements and laboratory studies: Bulletin of Volcanology, v. 73, p. 321–333, doi:10.1007/s00445-010-0411-6.

Manville, V., and Wilson, C.J.N., 2004, Vertical density currents: A review of their potential role in the deposition and interpretation of deep-sea ash layers: Journal of the Geological Society of London, v. 161, p. 947–958, doi:10.1144/0016-764903-067.

Manville, V., White, J.D.L., Houghton, B.F., and Wilson, C.J.N., 1998, The saturation behaviour of pumice and some sedimentological implications: Sedimentary Geology, v. 119, p. 5–16, doi:10.1016/S0037-0738(98)00057-8.

Manville, V., Segschneider, B., and White, J.D.L., 2002, Hydrodynamic behaviour of Taupo 1800a pumice: Implications for the sedimentology of remobilized pyroclasts: Sedimentology, v. 49, p. 955–976, doi:10.1046/j.1365-3091.2002.00485.x.

Manville, V., Németh, K., and Kano, K., 2010, Source to sink: A review of three decades of progress in the understanding of volcaniclastic processes, deposits, and hazards: Sedimentary Geology, v. 22, no. 3–4, p. 136–161.

Martín-Chivelet, J., Fregenal-Martínez, M.A., and Chacón, B., 2008, Traction structures in contourites, *in* Rebesco, M., and Camerlenghi, A., eds., Contourites: Amsterdam, Netherlands, Elsevier Science, p. 157–182, doi:10.1016/S0070-4571(08)10010-3.

Mastin, L.G., and Witter, J.B., 2000, The hazards of eruptions through lakes and seawater: Journal of Volcanology and Geothermal Research, v. 97, p. 195–214, doi:10.1016/S0377-0273(99)00174-2.

McPhie, J., Doyle, M., and Allen, R., 1993, Volcanic Textures: Hobart, Australia, ARC–Centre of Excellence in Ore Deposits, University of Tasmania, 198 p.

McPhie, J., and Allen, R.L., 2003, Submarine, silicic, syneruptive pyroclastic units in the Mount Read Volcanics, western Tasmania; influence of vent setting and proximity on lithofacies characteristics, *in* White, J.D.L., Smellie, J.L., and Clague, D.A., eds., Explosive Subaqueous Volcanism: Washington, D.C., American Geophysical Union, p. 245–258, doi:10.1029/140GM16.

Mills, A.A., 1984, Pillow lavas and the Leidenfrost effect: Journal of the Geological Society, v. 141, p. 183–186, doi:10.1144/gsjgs.141.1.0183.

Nishimura, A., 1991, Pliocene–Quaternary submarine pumice deposits in the Sumisu Rift area, Izu-Bonin arc, *in* Fisher, R.V., and Smith, G.A., eds., Sedimentation in Volcanic Settings: Tulsa, Oklahoma, Society for Sedimentary Geology, p. 201–208, doi:10.2110/pec.91.45.0201.

Paladio-Melosantos, M.L.O., Solidum, R.U., Scott, W.E., Quiambao, R.B., Umbal, J.V., Rodolfo, K.S., Tubianosa, B.S., de los Reyes, P.J., Alonso, R.A., and Ruelo, H.B., 1996, Tephra falls of the 1991 eruptions of Mount Pinatubo, *in* Newhall, C.G., and Punongbayan, R.S., eds., Fire and Mud; Eruptions and Lahars of Mount Pinatubo, Philippines: Quezon City, Philippine Institute of Volcanology and Seismology p. 513–536.

Piper, D.J.W., Cochonat, P., and Morrison, M.L., 1999, The sequence of events around the epicentre of the 1929 Grand Banks earthquake: Initiation of debris flows and turbidity current inferred from sidescan sonar: Sedimentology, v. 46, p. 79–97, doi:10.1046/j.1365-3091.1999.00204.x.

Rea, W.J., 1974, The volcanic geology and petrology of Montserrat, West Indies: Journal of the Geological Society of London, v. 130, no. 4, p. 341–366, doi:10.1144/gsjgs.130.4.0341.

Riggs, N.R., Ort, M.H., White, J.D.L., Wilson, C.J.N., Houghton, B.F., and Clarkson, R., 2001, Post–1.8-ka marginal sedimentation in Lake Taupo, New Zealand; effects of wave energy and sediment supply in a rapidly rising lake, *in* White, J.D.L., and Riggs, N.R., eds., Volcaniclastic Sedimentation in Lacustrine Settings: Oxford, UK, Blackwell Science, p. 151–177, doi:10.1002/9781444304251.ch8.

Risso, C., Scasso, R.A., and Aparicio, A., 2002, Presence of large pumice blocks on Tierra del Fuego and South Shetland Islands shorelines, from 1962 South Sandwich Islands eruption: Marine Geology, v. 186, p. 413–422, doi:10.1016/S0025-3227(02)00190-1.

Robertson, R.E.A., Aspinall, W.P., Herd, R.A., Norton, G.E., Sparks, R.S.J., and Young, S.R., 2000, The 1995–1998 eruption of the Soufrière Hills volcano, Montserrat, WI: Philosophical Transactions of the Royal Society, ser. A, Mathematical, Physical and Engineering Sciences, v. 358, p. 1619–1637, doi:10.1098/rsta.2000.0607.

Schindlbeck, J.C., Kutterolf, S., Freundt, A., Scudder, R.P., Pickering, K.T., and Murray, R.W., 2013, Emplacement processes of submarine volcaniclastic deposits (IODP Site C0011, Nankai Trough): Marine Geology, v. 343, p. 115–124, doi:10.1016/j.margeo.2013.06.017.

Self, S., 1992, Krakatau revisited: The course of events and interpretation of the 1883 eruption: GeoJournal, v. 28, p. 109–121, doi:10.1007/BF00177223.

Self, S., Rampino, M.R., Newton, M.S., and Wolff, J.A., 1984, Volcanological study of the great Tambora eruption of 1815: Geology, v. 12, p. 659–663, doi:10.1130/0091-7613(1984)12<659:VSOTGT>2.0.CO;2.

Sigurdsson, H., and Carey, S., 1989, Plinian and co-ignimbrite tephra fall from the 1815 eruption of Tambora volcano: Bulletin of Volcanology, v. 51, p. 243–270, doi:10.1007/BF01073515.

Sigurdsson, H., Sparks, R.S.J., Carey, S.N., and Huang, T.C., 1980, Volcanogenic sedimentation in the Lesser Antilles arc: The Journal of Geology, v. 88, p. 523–540, doi:10.1086/628542.

Sigurdsson, H.S., Cashdollar, S., and Sparks, R.S.J., 1982, The eruption of Vesuvius in A.D. 79: Reconstruction from historical and volcanological evidence: American Journal of Archaeology, v. 86, p. 39–51, doi:10.2307/504292.

Simkin, T., and Fiske, R.S., 1983, Krakatau 1883; the Volcanic Eruption and its Effects: Washington, D.C., Smithsonian Institute Press, 464 p.

Soule, A., and Carey, R.J., 2015, Mapping, Exploration and Sampling at Havre, Cruise RR 1506: Boston, Woods Hole Oceanographic Institution, 100 p.

Soulsby, R., 1997, Dynamics of Marine Sands; a Manual for Practical Applications: London, UK, Thomas Telford Publications, 249 p.

Sparks, R.S.J., Brazier, S., Huang, T.C., and Muerdter, D., 1983, Sedimentology of the Minoan deep-sea tephra layer in the Aegean and Eastern Mediterranean: Marine Geology, v. 54, p. 131–167, doi:10.1016/0025-3227(83)90011-7.

Stow, D.A.V., and Faugères, J.-C., 2008, Contourite facies and the facies model, *in* Rebesco, M., and Camerlenghi, A., eds., Contourites: Amsterdam, Netherlands, Elsevier Science, p. 223–256, doi:10.1016/S0070-4571(08)10013-9.

Sumner, E.J., Talling, P.J., Amy, L.A., Wynn, R.B., Stevenson, C.J., and Frenz, M., 2012, Facies architecture of individual basin-plain turbidites: Comparison with existing models and implications for flow processes: Sedimentology, v. 59, p. 1850–1887, doi:10.1111/j.1365-3091.2012.01329.x.

Swanson, S.E., and Kienle, J., 1988, The 1986 eruption of Mount St. Augustine; field test of a hazard evaluation: Journal of Geophysical Research, v. 93, p. 4500–4520, doi:10.1029/JB093iB05p04500.

Talling, P.J., Masson, D.G., Sumner, E.J., and Malgesini, G., 2012, Subaqueous sediment density flows: Depositional processes and deposit types: Sedimentology, v. 59, p. 1937–2003, doi:10.1111/j.1365-3091.2012.01353.x.

Tani, K., Fiske, R.S., Tamura, Y., Kido, Y., Naka, J., Shukuno, H., and Takeuchi, R., 2008, Sumisu volcano, Izu-Bonin arc, Japan: Site of a silicic caldera-forming eruption from a small open-ocean island: Bulletin of Volcanology, v. 70, p. 547–562, doi:10.1007/s00445-007-0153-2.

Taylor, B., Fujioka, K., et al., 1990, Proceeding of the Ocean Drilling Program Initial Reports 126: College Station, Texas, Ocean Drilling Program, doi:10.2973/odp.proc.ir.126.1990.

Taylor, R.N., Ishizuka, O., Michalik, A., Milton, J.A., and Croudace, I.W., 2015, Evaluating the precision of Pb isotope measurement by mass spectrometry: Journal of Analytical Atomic Spectrometry, v. 30, p. 198–213, doi:10.1039/C4JA00279B.

Trofimovs, J., Amy, L., Boudon, G., Deplus, C., Doyle, E., Fournier, N., Hart, M.B., Komorowski, J.C., Le Friant, A., Lock, E.J., Pudsey, C., Ryan, G., Sparks, R.S.J., and Talling, P.J., 2006, Submarine pyroclastic deposits formed at the Soufrière Hills volcano, Montserrat (1995–2003): What happens when pyroclastic flows enter the ocean?: Geology, v. 34, p. 549–552, doi:10.1130/G22424.1.

Trofimovs, J., Sparks, R.S.J., and Talling, P.J., 2008, Anatomy of a submarine pyroclastic flow and associated turbidity current: July 2003 dome collapse, Soufrière Hills volcano, Montserrat, West Indies: Sedimentology, v. 55, p. 617–634, doi:10.1111/j.1365-3091.2007.00914.x.

Trofimovs, J., Fisher, J.K., Macdonald, H.A., Talling, P.J., Sparks, R.S.J., Hart, M.B., Smart, C.W., Boudon, G., Deplus, C., Komorowski, J.C., Le Friant, A., Moreton, S.G., and Leng, M.J., 2010, Evidence for carbonate platform failure during rapid sea-level rise; ca 14 000 year old bioclastic flow deposits in the Lesser Antilles: Sedimentology, v. 57, p. 735–759, doi:10.1111/j.1365-3091.2009.01117.x.

Trofimovs, J., Foster, C., Sparks, R.S.J., Loughlin, S., Friant, A., Deplus, C., Porritt, L., Christopher, T., Luckett, R., Talling, P.J., Palmer, M.R., and Bas, T., 2012, Submarine pyroclastic deposits formed during the 20th May 2006 dome collapse of the Soufrière Hills volcano, Montserrat: Bulletin of Volcanology, v. 74, p. 391–405, doi:10.1007/s00445-011-0533-5.

Trofimovs, J., Talling, P.J., Fisher, J.K., Sparks, R.S.J., Watt, S.F.L., Hart, M.B., Smart, C.W., Le Friant, A., Cassidy, M., Moreton, S.G., and Leng, M.J., 2013, Timing, origin and emplacement dynamics of mass flows offshore of SE Montserrat in the last 110 ka; implications for landslide and tsunami hazards, eruption history, and volcanic island evolution: Geochemistry Geophysics Geosystems, v. 14, p. 385–406, doi:10.1002/ggge.20052.

Ui, T., 1973, Exceptionally far-reaching, thin pyroclastic flow in southern Kyushu, Japan: Bulletin of the Volcanological Society of Japan, v. 18, p. 153–168.

Valentine, P.C., Cooper, R.A., and Uzmann, J.R., 1984, Submarine sand dunes and sedimentary environments in Oceanographer Canyon: Journal of Sedimentary Petrology, v. 54, p. 704–715.

van Leuwenhock, A., 1704, Several microscopical observations on the pumice-stone, coral, spunges, etc.: Philosophical Transactions (1683–1775), v. 24, p. 2158–2163, doi:10.1098/rstl.1704.0105.

Vella, D., and Huppert, H.E., 2007, The waterlogging of floating objects: Journal of Fluid Mechanics, v. 585, p. 245–254, doi:10.1017/S002211200700715X.

Walker, G.P.L., 1972, Crystal concentration in ignimbrites: Contributions to Mineralogy and Petrology, v. 36, p. 135–146, doi:10.1007/BF00371184.

Walker, G.P.L., 1983, Ignimbrite types and ignimbrite problems: Journal of Volcanology and Geothermal Research, v. 17, p. 65–88, doi:10.1016/0377-0273(83)90062-8.

Walker, G.P.L., and Croasdale, R., 1971, Two Plinian-type eruptions in the Azores: Journal of the Geological Society of London, v. 127, p. 17–55, doi:10.1144/gsjgs.127.1.0017.

Wall-Palmer, D., Coussens, M., Talling, P.J., Jutzeler, M., Cassidy, M., Marchant, I., Palmer, M.R., Watt, S.F.L., Smart, C.W., Fisher, J.K., Hart, M.B., Fraass, A., Trofimovs, J., Le Friant, A., Ishizuka, O., Adachi, T., Aljahdali, M., Boudon, G., Breitkreuz, C., Endo, D., Fujinawa, A., Hatfield, R., Hornbach, M.J., Kataoka, K., Lafuerza, S., Maeno, F., Manga, M., Martinez-Colon, M., McCanta, M., Morgan, S., Saito, T., Slagle, A.L., Stinton, A.J., Subramanyam, K.S.V., Tamura, Y., Villemant, B., and Wang, F., 2014, Late Pleistocene stratigraphy of IODP Site U1396 and compiled chronology offshore of south and south west Montserrat, Lesser Antilles: Geochemistry Geophysics Geosystems, v. 15, p. 3000–3020, doi:10.1002/2014GC005402.

Watkins, N.D., Sparks, R.S.J., Sigurdsson, H., Huang, T.C., Federman, A., Carey, S., and Ninkovich, D., 1978, Volume and extent of the Minoan tephra from Santorini volcano: New evidence from deep-sea sediment cores: Nature, v. 271, p. 122–126, doi:10.1038/271122a0.

Watt, S.F.L., Talling, P.J., Vardy, M.E., Heller, V., Hühnerbach, V., Urlaub, M., Sarkar, S., Masson, D.G., Henstock, T.J., Minshull, T.A., Paulatto, M., Le Friant, A., Lebas, E., Berndt, C., Crutchley, G.J., Karstens, J., Stinton, A.J., and Maeno, F., 2012a, Combinations of

volcanic-flank and seafloor-sediment failure offshore Montserrat, and their implications for tsunami generation: Earth and Planetary Science Letters, v. 319–320, p. 228–240, doi:10.1016/j.epsl.2011.11.032.

Watt, S.F.L., Talling, P.J., Vardy, M.E., Masson, D.G., Henstock, T.J., Huehnerbach, V., Minshull, T.A., Urlaub, M., Lebas, E., Le Friant, A., Berndt, C., Crutchley, G.J., and Karstens, J., 2012b, Widespread and progressive seafloor-sediment failure following volcanic debris avalanche emplacement: Landslide dynamics and timing offshore Montserrat, Lesser Antilles: Marine Geology, v. 323–325, p. 69–94, doi:10.1016/j.margeo.2012.08.002.

Watt, S.F.L., Jutzeler, M., Talling, P.J., Carey, S.N., Sparks, R.S.J., Tucker, M., Stinton, A.J., Fisher, J.K., Wall-Palmer, D., Hühnerbach, V., and Moreton, S.G., 2015, New insights into landslide processes around volcanic islands from remotely operated vehicle (ROV) observations offshore Montserrat: Geochemistry Geophysics Geosystems, v. 16, p. 2240–2261, doi:10.1002/2015GC005781.

Wetzel, A., 2009, The preservation potential of ash layers in the deep-sea; the example of the 1991 Pinatubo ash in the South China Sea: Sedimentology, v. 56, p. 1992–2009, doi:10.1111/j.1365-3091.2009.01066.x.

White, J.D.L., 2000, Subaqueous eruption-fed density currents and their deposits: Precambrian Research, v. 101, p. 87–109, doi:10.1016/S0301-9268(99)00096-0.

White, J.D.L., and Houghton, B.F., 2006, Primary volcaniclastic rocks: Geology, v. 34, p. 677–680, doi:10.1130/G22346.1.

White, J.D.L., Manville, V., Wilson, C.J.N., Houghton, B.F., Riggs, N.R., and Ort, M., 2001, Settling and deposition of AD 181 Taupo pumice in lacustrine and associated environments, *in* White, J.D.L., and Riggs, N. R., eds., Volcaniclastic Sedimentation in Lacustrine Settings: Oxford, UK, Blackwell Science, p. 141–150, doi:10.1002/9781444304251.ch7.

Whitham, A.G., and Sparks, R.S.J., 1986, Pumice: Bulletin of Volcanology, v. 48, p. 209–223, doi:10.1007/BF01087675.

Wiesner, M.G., Yubo, W., and Lianfu, Z., 1995, Fallout of volcanic ash to the deep South China Sea induced by the 1991 eruption of Mount Pinatubo (Philippines): Geology, v. 23, p. 885–888, doi:10.1130/0091-7613(1995)023<0885:FOVATT>2.3.CO;2.

Wilson, C.J.N., 2001, The 26.5 ka Oruanui eruption, New Zealand: An introduction and overview: Journal of Volcanology and Geothermal Research, v. 112, p. 133–174, doi:10.1016/S0377-0273(01)00239-6.

Yokoyama, S., 1974, Mode of movement and emplacement of Ito pyroclastic flow from Aira caldera, Japan: Science Reports of the Tokyo Kyoiku Daigaku, Section C, Geology, Mineralogy and Geography, v. 12, p. 17–62.

Young, S.R., Sparks, R.S.J., Aspinall, W.P., Lynch, L.L., Miller, A.D., Robertson, R.E.A., and Shepherd, J.B., 1998, Overview of the eruption of Soufriere Hills volcano, Montserrat, 18 July 1995 to December 1997: Geophysical Research Letters, v. 25, p. 3389–3392, doi:10.1029/98GL01405.

Zellmer, G.F., Hawkesworth, C.J., Sparks, R.S.J., Thomas, L.E., Harford, C.L., Brewer, T.S., and Loughlin, S.C., 2003, Geochemical evolution of the Soufriere Hills volcano, Montserrat, Lesser Antilles volcanic arc: Journal of Petrology, v. 44, p. 1349–1374, doi:10.1093/petrology/44.8.1349.

Science Editor: Christian Koeberl
Associate Editor: Nancy Riggs

Manuscript Received 25 October 2015
Revised Manuscript Received 14 July 2016
Manuscript Accepted 14 August 2016

Printed in the USA